Nonclassical vibration analysis of piezoelectric nanosensor conveying viscous fluid

SAYYID H. HASHEMI KACHAPI
Department of Mechanical Engineering
Babol Noshirvani University of Technology
Shariati Street, Babol, Mazandaran 47148-71167
sha.hashemi.kachapi@gmail.com, IRAN

Abstract: - In this paper, the natural frequency, critical fluid velocity and stability analysis of piezoelectric biomedical nanosensor (PBMNS) based on cylindrical nanoshell conveying viscous fluid is investigated using the electro-elastic Gurtin–Murdoch surface/interface theory. This system subjected to nonlinear electrostatic field and viscoelastic medium including visco-pasternak and damping coefficients. Hamilton's principle and the assumed mode method combined with Euler – Lagrange is used for the governing equations and boundary conditions. It is shown that fluid velocity due to motion of biomarkers has major unpredictable effects on natural frequency and critical fluid velocity of the system and one should precisely consider their effects.
Key-Words: - Piezoelectric biomedical nanosensor, Natural frequency, Instability, Critical fluid velocity, Nanoshell, Gurtin–Murdoch surface/interface theory, Electrostatic force, Visco-Pasternak medium.

1 Introduction

Nanotechnology is a multidisciplinary branch of science which encompasses numerous diverse fields of science and technology, pharmaceutical, agricultural, environmental, advanced materials, chemical science, physics, electronics, information technology, and specially biomedical fields such as imaging agents, drug delivery vehicle, diagnostic tools, etc. to save human life along with other areas by application of engineering skills in surgical diagnosis, monitoring, treatment, and therapy etc. In recent years, the application of nanotechnology shows further advancement in several specific areas in biomedical such as drug targeting, bio-diagnostics, bioimaging, and genetic manipulation [1]. For example, in head and neck cancer (tumors) and breast cancer cells, image-guided laser ablation and photothermal therapy with laser light and plasmon naturals are the promising minimally invasive techniques currently being investigated as an alternative to conventional surgical interventions. For increase the conformality of therapy delivery, the use of tumortargeted nanoparticles, especially metallic nanoshell, which are preferentially targeted to the tumor and, thereby enhance the safety and efficacy of the overall procedure, are proposed [2-5]. For detection of a wide range of biomarkers such as cancer biomarkers many of materials such as carbon nanotubes, magnetic nanoparticles, gold nanoparticles and nanowires and other materials have been presented and developed [6]. Recently Gold nanoshells (AuNSs) and nanotube-based composite sensors have been intensively investigated and applied for medical application [7-11]. Also, a nanosensor is proposed for detection of cancer cells located in a particular region of a blood vessel [12] and for detection of cancer biomarkers in serum at ultralow concentrations [13]. Recently, a research project will lead to development of a new category of nanometer-sized chemical and biological sensors that are compatible with the intracellular environment and will enable new hypotheses to be tested in the role of metabolic coupling in pancreatic alpha cells and a range of other cellular systems involved in the regulation of normal human health [14]. With the development of material science, the piezoelectric nanosensor and nano actuator play an important role for medicine applications and have been fabricated as nano-beams, nano-plates, nano-membranes and nano-shells [15-17]. One of the most important scientific concepts in the design and fabrication of this nanosensor, and due to the high sensitivity that can be found in medical applications, is the analysis of dynamic and vibrations considering of nano-mechanical theories. Because of the large ratio of surface area to volume in nano-scaled structure, the behaviour of surfaces and interfaces lead to a significant factor in controlling the vibration analysis of piezoelectric Nano biomedical sensor based on nano-shell. In this case some non-classical

Acknowledgement

I highly appreciate the time and efforts of all the reviewers devoted to review my manuscript and I thank the Associate Editor and the reviewers for many helpful and constructive comments.

continuum theories such as the electro-elastic Gurtin–Murdoch surface elasticity theory have been introduced to develop the size-dependent continuum models [18-19]. In the past two decades, investigating the surface effects on the mechanical behavior of nanostructures has become one of the attractive research areas in nanomechanics, as evidenced by the large number of publications on this issue [20-25]. Recently, Zhu and Fang et al. studied free and forced vibration analysis of nano-sized single and double shell structures with piezoelectric layer based on GM surface/interface theory [20-21]. Ghorbanpour Arani et al. studied on vibration analysis of double walled visco-carbon nanotubes under magnetic fields [22]. In another research by Ghorbanpour Arani et al., nonlinear vibration of nano sheet with small scale and surface effects are investigated by using of nonlocal and surface piezoelasticity theories [23]. Also, vibration analysis of viscoelastic DWCNT unified with ZnO layers and subjected to magnetic and electric fields are studied by Fereidoon et al. [24]. Surface stress effect on the vibration of nanoscale pipes based on a size-dependent Timoshenko beam model is investigated by Ansari et al. [25]. Ye et al. presented a unified solution method for the free vibration analysis of composite shallow shells with general elastic boundary conditions [26]. Fazollari developed an analytical formulation for free vibration analysis of doubly curved laminated composite shallow shells by combining the dynamic stiffness method and a higher order shear deformation theory [27]. Mirza and Alizadeh investigated the effects of detached base length on the natural frequencies and modal shapes of cylindrical shells [28]. Loy et al. presented the free vibration analysis of cylindrical shells using an improved version of the differential quadrature method [29]. An analytical procedure to study the free vibration characteristics of thin circular cylindrical shells was presented by Naeem and Sharma, in which Ritz polynomial functions are used for solution of the problem [30]. Zeighampour et al. investigated wave propagation in viscoelastic single walled carbon nanotubes by accounting for the simultaneous effects of the nonlocal constant and the material length scale parameter and visco-Pasternak foundations [31].

In the present study, the natural frequency, critical fluid velocity and stability analysis of piezoelectric biomedical nanosensor (PBMNS) based on cylindrical nanoshell conveying viscous fluid is investigated using the electro-elastic Gurtin–Murdoch surface/interface theory and considering von-karman-Donnell's shell model. This system subjected to nonlinear electrostatic field, viscoelastic medium including visco-pasternak and damping coefficients. Hamilton's principle and also the assumed mode method combined with Euler – Lagrange is used for the governing equations, boundary conditions and for changing the partial differential equations into ordinary differential equations. Also stability analysis and dimensionless natural frequency ($\bar{\Omega}$) versus fluid velocity ($\bar{u}_f$) dimensionless of a piezoelectric biomedical nanosensor are accurately studied with respect to the different geometrical and material parameters.

2 Mathematical formulation

A piezoelectric biomedical nanosensor shown in Figure 1 based on cylindrical nanoshell embedded with a visco-Pasternak medium and electrostatic force with incoming bloodstream as viscous fluid.

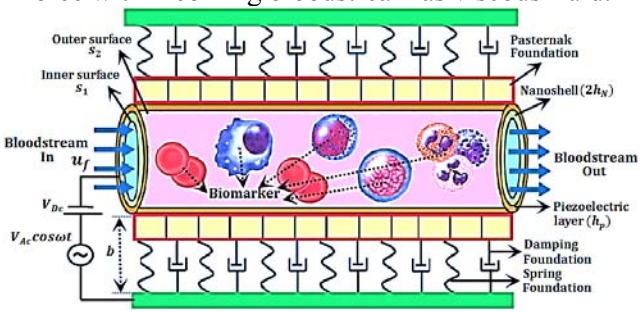

Fig. 1. Piezoelectric biomedical nanosensor (PBMNS) conveying viscous bloodstream

The length of nano shell is L, the geometrical parameters of the cylindrical shell are mid-surface radius R, thickness of cylindrical shell $2h_N$ thickness of piezoelectric material layer h_p. With the origin of coordinate system located on the middle surface of nano-shell, the coordinates of a typical point in the axial, circumferential and radius directions are described by x, θ, and z, respectively. Also, K_w ,K_p and C_w are stiffness coefficient of Winkler foundation, shear layer of Pasternak foundation and the damping factor of the visco medium for the transverse motion, respectively. Young modulus, Poisson ratio and the mass density of cylindrical nano-shell represent E_N, υ_N and ρ_N, respectively. In the present nano-shell, it is assumed that the mention material properties vary through the thickness of nano-shell according to the power-law function. They are written as

$$E_N = (E_T - E_B)\left(\frac{2z + h_N}{2h_N}\right)^q + E_B \quad (1)$$

$$\upsilon_N = (\upsilon_T - \upsilon_B)\left(\frac{2z + h_N}{2h_N}\right)^q + \upsilon_B \quad (2)$$

$$\rho_N = (\rho_T - \rho_B)\left(\frac{2z + h_N}{2h_N}\right)^q + \rho_B \quad (3)$$

where q is the power-law exponent. The subscripts T and B represent the properties of the nano-shell at the upper and lower layers, respectively.

Young modulus, Poisson ratio, piezoelectric and dielectric constants and the mass density of piezoelectric layer are $E_p, \upsilon_p, e_{31p}, e_{32p}, \eta_{33p}$ and ρ_p. Due to the nano-sized property, the ratio of surface to the volume becomes large, and the surface energy around the shell expresses significant effect on the vibration of nano-structure. According to the electro-elastic surface/interface theory, the surface/interface region adhered to the neigh boring solids is several atomic sizes, and has its own electromechanical properties. The surface at the outer piezoelectric layer is denoted by s_2, and the inner surface is denoted by s_1, as shown in Fig. 1. The material properties of surface s_2 are Lamé's constants λ^{s_2}, μ^{s_2}, residual stress $\tau_0^{s_2}$ and piezoelectric constants $e_{31p}^{s_2}, e_{32p}^{s_2}$. Those of the inner surface are Lamé's constants λ^{s_1}, μ^{s_1}, and residual stress $\tau_0^{s_1}$.

Due to the character of nano-shell, the state of generalized plane stress of shells is assumed, and the normal stress in the radial direction is zero. In the cylindrical nano-shell, the constitutive relation can be expressed as [32, 33];

$$\begin{Bmatrix}\sigma_{xxN}\\ \sigma_{\theta\theta N}\\ \tau_{x\theta N}\end{Bmatrix} = \begin{bmatrix}C_{11N} & C_{12N} & 0\\ C_{21N} & C_{22N} & 0\\ 0 & 0 & C_{66N}\end{bmatrix}\begin{Bmatrix}\varepsilon_{xx}\\ \varepsilon_{\theta\theta}\\ \gamma_{x\theta}\end{Bmatrix}, \quad (4)$$

$$or \quad \{\sigma_N\} = [C_N]\{\varepsilon\},$$

In the outside piezoelectric shell, the constitutive relation can be expressed as [17]

$$\begin{Bmatrix}\sigma_{xxp}\\ \sigma_{\theta\theta p}\\ \tau_{x\theta p}\end{Bmatrix} = \begin{bmatrix}C_{11p} & C_{12p} & 0\\ C_{21p} & C_{22p} & 0\\ 0 & 0 & C_{66p}\end{bmatrix}\begin{Bmatrix}\varepsilon_{xx}\\ \varepsilon_{\theta\theta}\\ \gamma_{x\theta}\end{Bmatrix} - \begin{bmatrix}0 & 0 & e_{31p}\\ 0 & 0 & e_{32p}\\ 0 & 0 & 0\end{bmatrix}\begin{Bmatrix}\bar{E}_{xp}\\ \bar{E}_{\theta p}\\ \bar{E}_{zp}\end{Bmatrix}, \quad (5)$$

$$\text{or} \quad \{\sigma_p\} = [C_p]\{\varepsilon\} - [e_p]\{\bar{E}_p\},$$

In which the subscripts N and P represent the cylindrical nano-shell and piezoelectric layers, respectively. $\{\bar{E}_p\}$ is the vector of electric field for piezoelectric layers. $[C_N]$ and $[C_p]$are the matrixes of elastic constants, and they can be denoted as

$$C_{11N} = \frac{E_N}{1-\upsilon_N^2} = C_{22N}, \quad C_{12N} = \frac{\upsilon_N E_N}{1-\upsilon_N^2} = C_{21N}, C_{66N} = \frac{E_N}{2(1+\upsilon_N)} \quad (6)$$

$$C_{11p} = \frac{E_p}{1-\upsilon_p^2} = C_{22p}, \quad C_{12p} = \frac{\upsilon_p E_p}{1-\upsilon_p^2} = C_{21p}, \quad C_{66p} = \frac{E_p}{2(1+\upsilon_p)} \quad (7)$$

Since the piezoelectric layers are very thin, $\bar{E}_{xp}$and $\bar{E}_{\theta p}$are assumed to be zero ($\bar{E}_{xp} = \bar{E}_{\theta p} = 0$), and only the radial component of electric field $\bar{E}_{zp}$ is considered. Consequetly, $\{\bar{E}_p\}$ can be written as [34]

$$\begin{Bmatrix}\bar{E}_{xp}\\ \bar{E}_{\theta p}\\ \bar{E}_{zp}\end{Bmatrix} = \begin{Bmatrix}0\\ 0\\ V_p/h_p\end{Bmatrix}, \quad (8)$$

where V_p is the voltage applied to piezoelectric layers. In addition, the voltages at the piezoelectric surface $S_2(z = h_N + h_p)$ and $S_1(z = h_N)$ are $+V_p$ and $-V_p$, respectively. Based on these assumptions mentioned above, the radial component of electric displacement D_{zp} can be presented as

$$D_{zp} = e_{31p}\varepsilon_{xx} + e_{32p}\varepsilon_{\theta\theta} + \eta_{33p}\bar{E}_{zp} \quad (9)$$

3 Non- classical Shell theory

Within the framework of classical shell theory, the displacement fields of the nano-shell can be written as

$$u_x(x,\theta,z) = u(x,\theta) - z\frac{\partial w(x,\theta)}{\partial x}, \quad (10)$$

$$u_\theta(x,\theta,z) = v(x,\theta) - \frac{z}{R}\frac{\partial w(x,\theta)}{\partial \theta}, \quad (11)$$

$$u_z(x,\theta,z) = w(x,\theta), \quad (12)$$

where u, v and w stand for the middle surface displacements in the x , θ and z directions, respectively. The nonlinear deflection and curvatures are defined by von-karman-Donnell's theory as [32, 33]

$$\begin{Bmatrix}\varepsilon_{xx}\\ \varepsilon_{\theta\theta}\\ \gamma_{x\theta}\end{Bmatrix} = \begin{Bmatrix}\varepsilon_{xx}^0\\ \varepsilon_{\theta\theta}^0\\ \gamma_{x\theta}^0\end{Bmatrix} + z\begin{Bmatrix}\kappa_{xx}\\ \kappa_{\theta\theta}\\ \kappa_{x\theta}\end{Bmatrix} = \begin{Bmatrix}\dfrac{\partial u}{\partial x} + \dfrac{1}{2}\left(\dfrac{\partial w}{\partial x}\right)^2\\ \dfrac{1}{R}\left(\dfrac{\partial v}{\partial \theta} + w\right) + \dfrac{1}{2R^2}\left(\dfrac{\partial w}{\partial \theta}\right)^2\\ \dfrac{1}{R}\dfrac{\partial u}{\partial \theta} + \dfrac{\partial v}{\partial x} + \dfrac{1}{R}\dfrac{\partial w}{\partial x}\dfrac{\partial w}{\partial \theta}\end{Bmatrix} \quad (13)$$

$$-z\begin{Bmatrix}\dfrac{\partial^2 w}{\partial x^2}\\ \dfrac{1}{R^2}\dfrac{\partial^2 w}{\partial \theta^2}\\ \dfrac{2}{R}\dfrac{\partial^2 w}{\partial x \partial \theta}\end{Bmatrix}$$

in which ε^0_{xx} ،$\varepsilon^0_{\theta\theta}$ and $\gamma^0_{x\theta}$ are the middle surface strains, and κ_{xx} ,$\kappa_{\theta\theta}$ and $\kappa_{x\theta}$ are the curvature components of the nano-shell.

Since the dimension of the shell is at nanometer scale, the surface effect needs to be considered. On based of the Gurtin–Murdoch surface elasticity theory, the constitute relations for surfaces can be written as [18-20]

$$\sigma^{s_2}_{\alpha\beta} = \tau_0^{s_2}\delta_{\alpha\beta} + \left(\tau_0^{s_2} + \lambda^{s_2}\right)\varepsilon_{qq}\delta_{\alpha\beta} \quad (14)$$
$$+2\left(\mu^{s_2} - \tau_0^{s_2}\right)\varepsilon_{\alpha\beta}$$
$$+\tau_0^{s_2}u^{s_2}_{\alpha,\beta} - e_p^{s_2}E_{zp}, \sigma^{s_2}_{\alpha z} = \tau_0^{s_2}u^{s_2}_{z,\alpha}, \quad \sigma^{s_1}_{\alpha z} =$$
$$\tau_0^{s_1}u^{s_1}_{z,\alpha}, (\alpha,\beta = x,\theta)$$
$$\sigma^{s_1}_{\alpha\beta} = \tau_0^{s_1}\delta_{\alpha\beta} + \left(\tau_0^{s_1} + \lambda^{s_1}\right)\varepsilon_{qq}\delta_{\alpha\beta}$$
$$+2\left(\mu^{s_1} - \tau_0^{s_1}\right)\varepsilon_{\alpha\beta} + \tau_0^{s_1}u^{s_1}_{\alpha,\beta},$$

in which $\delta_{\alpha\beta}$ is the Kronecker delta function. Furthermore, the components of stress at the surfaces can be expressed as

$$\sigma^{s_2}_{xx} = (\lambda^{s_2} + 2\mu^{s_2})\varepsilon_{xx} + \left(\tau_0^{s_2} + \lambda^{s_2}\right)\varepsilon_{\theta\theta} \quad (15)$$
$$-\frac{\tau_0^{s_2}}{2}\left(\frac{\partial w}{\partial x}\right)^2 + \tau_0^{s_2} - e^{s_2}_{31p}E_{zp},$$
$$\sigma^{s_2}_{\theta\theta} = \left(\tau_0^{s_2} + \lambda^{s_2}\right)\varepsilon_{xx} + (\lambda^{s_2} + 2\mu^{s_2})\varepsilon_{\theta\theta}$$
$$-\tau_0^{s_2}\left(\frac{w}{R} + \frac{1}{2R^2}\left(\frac{\partial w}{\partial \theta}\right)^2\right) + \tau_0^{s_2} - e^{s_2}_{32p}E_{zp},$$
$$\sigma^{s_1}_{xx} = (\lambda^{s_1} + 2\mu^{s_1})\varepsilon_{xx} + \left(\tau_0^{s_1} + \lambda^{s_1}\right)\varepsilon_{\theta\theta}$$
$$-\frac{\tau_0^{s_1}}{2}\left(\frac{\partial w}{\partial x}\right)^2 + \tau_0^{s_1},$$
$$\sigma^{s_1}_{\theta\theta} = \left(\tau_0^{s_1} + \lambda^{s_1}\right)\varepsilon_{xx} + (\lambda^{s_1} + 2\mu^{s_1})\varepsilon_{\theta\theta}$$
$$-\tau_0^{s_1}\left(\frac{w}{R} + \frac{1}{2R^2}\left(\frac{\partial w}{\partial \theta}\right)^2\right) + \tau_0^{s_1}$$
$$\sigma^{s_i}_{x\theta} = \mu^{s_i}\gamma_{x\theta} - \tau_0^{s_i}\begin{pmatrix}\dfrac{\partial v}{\partial x} + \dfrac{1}{2R}\dfrac{\partial w}{\partial x}\dfrac{\partial w}{\partial \theta}\\ -\dfrac{z}{R}\dfrac{\partial^2 w}{\partial x \partial \theta}\end{pmatrix},$$
$$\sigma^{s_i}_{xz} = \tau_0^{s_i}\frac{\partial w}{\partial x},$$
$$\sigma^{s_i}_{\theta x} = \mu^{s_i}\gamma_{x\theta} - \tau_0^{s_i}\begin{pmatrix}\dfrac{1}{R}\dfrac{\partial u}{\partial \theta} + \dfrac{1}{2R}\dfrac{\partial w}{\partial x}\dfrac{\partial w}{\partial \theta}\\ -\dfrac{z}{R}\dfrac{\partial^2 w}{\partial x \partial \theta}\end{pmatrix},$$
$$\sigma^{s_i}_{\theta z} = \frac{\tau_0^{s_i}}{R}\frac{\partial w}{\partial \theta}, (i = 1,2)$$

Based on the classical continuum models, σ_{zz} is neglected due to its small value as compared to other normal stress components. But, in the present nonclassical continuum model, this assumption does not satisfy the surface conditions. Thus, it is supposed that σ_{zz} varies linearly through the thickness and satisfies the balance conditions on the surfaces [35, 36], i.e.

$$\sigma_{zz} = \frac{1}{2}\begin{pmatrix}\left(\dfrac{\partial \sigma^{s_2}_{xz}}{\partial x} + \dfrac{1}{R}\dfrac{\partial \sigma^{s_2}_{\theta z}}{\partial \theta} - \rho^{s_2}\dfrac{\partial^2 w}{\partial t^2}\right)\\ -\left(\dfrac{\partial \sigma^{s_1}_{xz}}{\partial x} + \dfrac{1}{R}\dfrac{\partial \sigma^{s_1}_{\theta z}}{\partial \theta} - \rho^{s_1}\dfrac{\partial^2 w}{\partial t^2}\right)\end{pmatrix} \quad (16)$$
$$+\frac{1}{2h_N + h_p}\begin{pmatrix}\left(\dfrac{\partial \sigma^{s_2}_{xz}}{\partial x} + \dfrac{1}{R}\dfrac{\partial \sigma^{s_2}_{\theta z}}{\partial \theta} - \rho^{s_2}\dfrac{\partial^2 w}{\partial t^2}\right)\\ +\left(\dfrac{\partial \sigma^{s_1}_{xz}}{\partial x} + \dfrac{1}{R}\dfrac{\partial \sigma^{s_1}_{\theta z}}{\partial \theta} - \rho^{s_1}\dfrac{\partial^2 w}{\partial t^2}\right)\end{pmatrix}$$

For simplification, the material properties of surfaces and interfaces are selected as

$$\tau_0^{s_1} = \tau_0^{s_2} = \tau_0^s, \ \lambda^{s_1} = \lambda^{s_2} = \lambda^s,$$
$$\mu^{s_1} = \mu^{s_2} = \mu^s, \ e^{s_2}_{31p} = e^s_{31p}, \quad (17)$$
$$e^{s_2}_{32p} = e^s_{32p}$$

By means of Eqs. (15) and (16), σ_{zz} can be rewritten as

$$\sigma_{zz} = \begin{pmatrix}\dfrac{\left(\tau_0^{s_2} - \tau_0^{s_1}\right)}{2}\\ +\dfrac{z\left(\tau_0^{s_2} + \tau_0^{s_1}\right)}{2h_N + h_p}\end{pmatrix}\begin{pmatrix}\dfrac{\partial^2 w}{\partial x^2}\\ +\dfrac{1}{R^2}\dfrac{\partial^2 w}{\partial \theta^2}\end{pmatrix} \quad (18)$$
$$+\left(\frac{\left(\rho^{s_1} - \rho^{s_2}\right)}{2} - \frac{z\left(\rho^{s_1} + \rho^{s_2}\right)}{2h_N + h_p}\right)\frac{\partial^2 w}{\partial t^2},$$

According to Eq. (18), the normal stresses σ_{xx} and $\sigma_{\theta\theta}$ Eqs. (4) and (5) can be rewrite ten as

$$\sigma_{xxN} = C_{11N}\varepsilon_{xx} + C_{12N}\varepsilon_{\theta\theta} + \frac{\upsilon_N\sigma_{zz(N,p)}}{1 - \upsilon_N}, \quad (19a)$$

$$\sigma_{\theta\theta N} = C_{21N}\varepsilon_{xx} + C_{22N}\varepsilon_{\theta\theta} + \frac{\upsilon_N\sigma_{zz(N,p)}}{1 - \upsilon_N}, \quad (19b)$$

$$\sigma_{x\theta N} = C_{66N}\gamma_{x\theta}, \quad (19c)$$

$$\sigma_{xxp} = C_{11p}\varepsilon_{xx} + C_{12p}\varepsilon_{\theta\theta} - e_{31p}\bar{E}_{xp} + \frac{\upsilon_p\sigma_{zz(N,p)}}{1 - \upsilon_p}, \quad (19d)$$

$$\sigma_{\theta\theta p} = C_{21p}\varepsilon_{xx} + C_{22p}\varepsilon_{\theta\theta} - e_{32p}\bar{E}_{\theta p} + \frac{\upsilon_N\sigma_{zz(N,p)}}{1 - \upsilon_p}, \quad (19e)$$

$$\sigma_{x\theta p} = C_{66p}\gamma_{x\theta}, \quad (19f)$$

4 Governing equations

In this section, the governing equations of motion of the piezoelectric cylindrical nanoshell are obtained by applying the assumed mode method.

The total strain and kinetic energies considering the surface stress effect are expressed as:

$$\begin{aligned}\pi &= \frac{1}{2}\int_0^L\int_0^{2\pi}\int_{-h_N}^{h_N}\left(\sigma_{ijN}\varepsilon_{ij}\right)Rdzd\theta dx\\ &+\frac{1}{2}\int_0^L\int_0^{2\pi}\int_{h_N}^{h_N+h_p}\begin{pmatrix}\sigma_{ijp}\varepsilon_{ij}\\ -\bar{E}_{zp}D_{zp}\end{pmatrix}Rdzd\theta dx\\ &+\frac{1}{2}\int_0^L\int_0^{2\pi}\begin{pmatrix}\sigma_{ij}^{s_2}\varepsilon_{ij}\\ -\bar{E}_{zp}D_i^{s_2}\end{pmatrix}\begin{pmatrix}R+h_N\\ +h_p\end{pmatrix}d\theta dx\\ &+\frac{1}{2}\int_0^L\int_0^{2\pi}\left(\sigma_{ij}^{s_1}\varepsilon_{ij}\right)(R-h_N)d\theta dx\\ &=\frac{1}{2}\int_0^L\int_0^{2\pi}\begin{Bmatrix}N_{xx}\varepsilon_{xx}^0+N_{\theta\theta}\varepsilon_{\theta\theta}^0\\ +N_{x\theta}\gamma_{x\theta}^0+M_{xx}\kappa_{xx}\\ +M_{\theta\theta}\kappa_{\theta\theta}+M_{x\theta}\kappa_{x\theta}\\ +\eta_{33}\bar{E}_{zp}^2h_p\end{Bmatrix}Rd\theta dx\,.\end{aligned} \tag{20}$$

$$T=\frac{1}{2}\iint\left\{I\begin{pmatrix}\left(\frac{\partial u}{\partial t}\right)^2+\left(\frac{\partial v}{\partial t}\right)^2\\ +\left(\frac{\partial w}{\partial t}\right)^2\end{pmatrix}\right\}Rd\theta dx \tag{21}$$

where

$$\begin{aligned}I&=\int_{-h_N}^{h_N}\rho_N\,dz+\int_{h_N}^{h_N+h_p}\rho_p\,dz+\rho^s\\ &=2\rho_Nh_N+\rho_ph_p+\rho^{s_2}|_{z=-h_N}\\ &+\rho^{s_1}|_{z=h_N+h_p}\end{aligned} \tag{22}$$

Which ρ_N, ρ_p and ρ^s are the mass density of nanoshell, piezoelectric layer and surfaces, respectively.

In Eq. (20), the stresses and moment resultants are defined in appendix A.

The work done by the surrounded viscoelastic medium including the visco-Pasternak medium and viscous damping and the electrostatic force can be written as [37-39]

$$W_{vm}=-\int_0^L\int_0^{2\pi}\left\{\begin{pmatrix}K_ww\\ -K_p\nabla^2w\\ +C_w\left(\frac{\partial w}{\partial t}\right)\end{pmatrix}w\right\}Rd\theta dx \tag{23}$$

$$W_e=\int_0^L\int_0^{2\pi}\begin{pmatrix}\frac{\pi\Upsilon(V_{DC}+V_{AC}\cos(\omega t))^2}{\left(\sqrt{(b-w)\times\begin{pmatrix}2R+b\\ -w\end{pmatrix}}\right)\times}\\ \left[\cosh^{-1}\left(1+\frac{b-w}{R}\right)\right]^2\end{pmatrix}w\,Rd\theta dx \tag{24}$$

For electrostatic force, b, R and $\Upsilon = 8.85\times 10^{-12}C^2N^{-1}m^{-2}$, respectively, are electrode distance to nanoshell, nanoshell radius and the air permittivity [39].

The equation for the fluid (in this paper, bloodstream) motion may be described by the well-known Navier–Stokes equation as [40]

$$\rho_f\frac{DV}{Dt}=-\nabla P+\mu\nabla^2V+F_{body}, \tag{25}$$

where V ≡ (v_x, v_z, v_z) is the flow velocity vector in cylindrical coordinate system with components in z, θ, and r directions. This vector can be expressed as follows

$$v_x=\frac{\partial u}{\partial t}+u_f\cos(\theta), \tag{26a}$$

$$v_\theta=\frac{\partial v}{\partial t}, \tag{26b}$$

$$v_z=\frac{\partial w}{\partial t}-u_f\sin(\theta), \tag{26c}$$

Where $\theta=-\frac{\partial w}{\partial x}$ and u_f is the constant velocity of the fluid (blood). Also P, μ, and ρ_f are the pressure, the effective fluid viscosity, and the mass density of the fluid, respectively, and F_{body} represents the body forces. Furthermore, ∇ and ∇^2 are gradient and Laplasian operators, respectively and $\frac{D}{Dt}$ is perfect derivative which can be defined as below:

$$\frac{D}{Dt}=\frac{\partial}{\partial t}+v_x\frac{\partial}{\partial x}+v_\theta\frac{\partial}{\partial\theta}+v_z\frac{\partial}{\partial z}, \tag{27}$$

Substituting Eqs. (26) and (27) into (25) we obtain the pressure of fluid as:

$$\begin{aligned}\frac{\partial P_z}{\partial z}&=-\rho_f\left(\frac{\partial^2w}{\partial t^2}+2u_f\frac{\partial^2w}{\partial x\partial t}+u_f^2\frac{\partial^2w}{\partial x^2}\right)\\ &+\mu\begin{pmatrix}\frac{\partial^3w}{\partial x^2\partial t}+\frac{\partial^3w}{R^2\partial\theta^2\partial t}\\ +u_f\left(\frac{\partial^3w}{\partial x^3}+\frac{\partial^3w}{R^2\partial\theta^2\partial x}\right)\end{pmatrix}.\end{aligned} \tag{28}$$

With multiple both side of above equation at the cross-sectional area of the internal fluid (A_f), radial force is expressed as:

$$\begin{aligned}F_{fluid}&=A_f\frac{\partial P}{\partial r}\\ &=-\rho_fA_f\begin{pmatrix}\frac{\partial^2w}{\partial t^2}+2u_f\frac{\partial^2w}{\partial x\partial t}\\ +u_f^2\frac{\partial^2w}{\partial x^2}\end{pmatrix}\\ &+\mu_fA_f\begin{pmatrix}\frac{\partial^3w}{\partial x^2\partial t}+\frac{\partial^3w}{R^2\partial\theta^2\partial t}\\ +u_f\left(\frac{\partial^3w}{\partial x^3}+\frac{\partial^3w}{R^2\partial\theta^2\partial x}\right)\end{pmatrix}.\end{aligned} \tag{29}$$

Considering the slip boundary condition in the analysis for exact investigation of the behaviour of the nanoflow, the average velocity correction factor VCF is introduced to establish the relation between slip average velocity V_{slip} and no-slip average velocity $V_{no-slip}$, i.e.;

$$u_f = V_{slip} = VCF \times V_{no-slip}, \tag{30}$$

where VCF coefficient can be written as [40]:

$$VCF = (1 + \alpha k_n)\left[+4\left(\frac{2-\sigma_v}{\sigma_v}\right)\left(\frac{k_n}{1+k_n}\right)\right], \tag{31}$$

where the slip of flow from inner nanotube through Knudsen number (k_n) is considered and for practical purposes, the tangential momentum accommodation coefficient $\sigma_v = 0.7$. Other parameters are:

$$\alpha = \frac{2\alpha_0}{\pi}[tan^{-1}(a_1 k_n^B)],$$
$$\alpha_0 = \frac{64}{3\pi\left(1-\frac{4}{b_1}\right)}, \tag{32}$$

Where $a_1 = 4$ and $B = 0.4$. And also for slip boundary condition, the value of parameter b_1 is set to be $b_1 = -1$. Hence, the external work of the fluid can be expressed as:

$$W_f = \int_0^L \int_0^{2\pi} F_{fluid}\, w\, R d\theta dx$$
$$= \int_0^L \int_0^{2\pi} \left\{ \begin{array}{l} -\rho_f A_f \left(\begin{array}{c} \frac{\partial^2 w}{\partial t^2} + \\ 2\left(\begin{matrix} VCF \times \\ V_{no-slip} \end{matrix}\right) \times \\ \frac{\partial^2 w}{\partial x \partial t} + \\ \left(\begin{matrix} VCF \times \\ V_{no-slip} \end{matrix}\right)^2 \times \\ \frac{\partial^2 w}{\partial x^2} \end{array} \right) \\ +\mu A_f \left(\begin{array}{c} \frac{\partial^3 w}{\partial x^2 \partial t} + \\ \frac{\partial^3 w}{R^2 \partial \theta^2 \partial t} + \\ \left(\begin{matrix} VCF \times \\ V_{no-slip} \end{matrix}\right) \times \\ \left(\begin{array}{c} \frac{\partial^3 w}{\partial x^3} + \\ \frac{\partial^3 w}{R^2 \partial x \partial \theta^2} \end{array} \right) \end{array} \right) \end{array} \right\} w\, R d\theta dx R d \tag{33}$$

The equations of motion and corresponding boundary conditions of the piezoelectric shell can be derived from Hamilton's principle

(34)

There are two ways to obtain the equations of motion for a mechanical system: Hamilton's principle and Euler–Lagrange equation. Hamilton's principle is the main procedure to obtain the equations of motion and boundary conditions. The equations of motion and corresponding boundary conditions of the piezoelectric nano shell can be derived from Hamilton's principle and by taking the variations of displacements u, v and w, and integrating by parts, and by equating the coefficients of δu, δv and δw to zero, the governing equations of motion are derived as:

$$\delta u: \quad \frac{\partial N_{xx}}{\partial x} + \frac{1}{R}\frac{\partial N_{x\theta}}{\partial \theta} = I\frac{\partial^2 u}{\partial t^2}, \tag{35}$$

$$\delta v: \quad \frac{\partial N_{x\theta}}{\partial x} + \frac{1}{R}\frac{\partial N_{\theta\theta}}{\partial \theta} = I\frac{\partial^2 v}{\partial t^2}, \tag{36}$$

$$\begin{aligned} \delta w: \ & \frac{\partial^2 M_{xx}}{\partial x^2} + \frac{2}{R}\frac{\partial^2 M_{x\theta}}{\partial x \partial \theta} + \frac{1}{R^2}\frac{\partial^2 M_{\theta\theta}}{\partial \theta^2} - \frac{N_{\theta\theta}}{R} \\ & + N_{xx}\frac{\partial^2 w}{\partial x^2} + \frac{\partial N_{xx}}{\partial x}\frac{\partial w}{\partial x} + \frac{N_{\theta\theta}}{R^2}\frac{\partial^2 w}{\partial \theta^2} + \frac{1}{R^2}\frac{\partial N_{\theta\theta}}{\partial \theta}\frac{\partial w}{\partial \theta} \\ & + \frac{2}{R}N_{x\theta}\frac{\partial^2 w}{\partial x \partial \theta} + \frac{1}{R}\frac{\partial N_{x\theta}}{\partial x}\frac{\partial w}{\partial \theta} + \frac{1}{R}\frac{\partial N_{x\theta}}{\partial \theta}\frac{\partial w}{\partial x} \\ & = I\frac{\partial^2 w}{\partial t^2} + C_w\frac{\partial w}{\partial t} + K_w w - K_p \nabla^2 w \\ & - \left[\begin{array}{c} -\rho_f A_f \left(\begin{array}{c} \frac{\partial^2 w}{\partial t^2} \\ +2(VCF \times V_{no-slip})\frac{\partial^2 w}{\partial x \partial t} + \\ \left(VCF \times V_{no-slip}\right)^2 \frac{\partial^2 w}{\partial x^2} \end{array} \right) \\ +\mu A_f \left(\begin{array}{c} \frac{\partial^3 w}{\partial x^2 \partial t} + \frac{\partial^3 w}{R^2 \partial \theta^2 \partial t} + \\ (VCF \times V_{no-slip}) \times \\ \left(\frac{\partial^3 w}{\partial x^3} + \frac{\partial^3 w}{R^2 \partial \theta^2 \partial x}\right) \end{array} \right) \end{array} \right] \\ & - \frac{\pi \Upsilon (V_{DC} + V_{AC}\cos(\omega t))^2}{\sqrt{(b-w)\times(2R+b-w)}\left[\cosh^{-1}\left(1+\frac{b-w}{R}\right)\right]^2}, \end{aligned} \tag{37}$$

and boundary conditions are obtained as follows:

$$\delta u = 0 \quad or \quad N_{xx}n_x + \frac{1}{R}N_{x\theta}n_\theta = 0, \tag{38a}$$

$$\delta v = 0 \quad or \quad N_{x\theta}n_x + \frac{1}{R}N_{\theta\theta}n_\theta = 0, \tag{38b}$$

$$\begin{aligned} \delta w = 0 \ \ or \ & \left(\begin{array}{c} \frac{\partial M_{xx}}{\partial x} + \frac{1}{R}\frac{\partial M_{x\theta}}{\partial \theta} \\ +N_{xx}\frac{\partial w}{\partial x} + \frac{N_{x\theta}}{R}\frac{\partial w}{\partial \theta} \end{array} \right) n_x \\ & + \left(\begin{array}{c} \frac{1}{R}\frac{\partial M_{x\theta}}{\partial x} + \frac{1}{R^2}\frac{\partial M_{\theta\theta}}{\partial \theta} \\ +\frac{N_{x\theta}}{R}\frac{\partial w}{\partial x} + \frac{N_{\theta\theta}}{R^2}\frac{\partial w}{\partial \theta} \end{array} \right) n_\theta = 0, \end{aligned} \tag{38c}$$

$$\frac{\partial w}{\partial x}=0 \quad or \quad M_{xx}n_x+\frac{1}{R}M_{x\theta}n_\theta=0, \tag{38d}$$

$$\frac{\partial w}{\partial \theta}=0 \quad or \quad \frac{1}{R}M_{x\theta}n_x+\frac{1}{R^2}M_{\theta\theta}n_\theta=0, \tag{38e}$$

But Euler–Lagrange method is an easier way to obtain the equations of motion. The resulting equations can be solved by the assumed mode method. In the assumed modes method, the admissible functions must satisfy the geometric boundary conditions and there is no need to satisfy the natural boundary conditions. Hence, solving the equations with this method reduces significantly the complexity of the problem. Therefore, in this work, the assumed mode method is used to obtain the equations of motion using Euler–Lagrange method. Following dimensionless parameters are used:

$$\bar{u}=\frac{u}{h_N},\bar{v}=\frac{v}{h_N},\bar{w}=\frac{w}{h_N},\xi=\frac{x}{L},\bar{b}=\frac{b}{h_N},$$
$$\bar{A}_{ijN}=\frac{A_{ijN}}{A_{11N}},\bar{B}_{ijN}=\frac{B_{ijN}}{A_{11N}h_N},$$
$$\bar{D}_{ijN}=\frac{D_{ijN}}{A_{11N}h_N^2},\bar{A}_{ijp}=\frac{A_{ijp}}{A_{11N}},$$
$$\bar{A}^*_{ij}=\frac{A^*_{ij}}{A_{11N}},\bar{B}_{ijp}=\frac{B_{ijp}}{A_{11N}h_N},$$
$$\bar{B}^*_{ij}=\frac{B^*_{ij}}{A_{11N}h_N},\bar{D}_{ijp}=\frac{D_{ijp}}{A_{11N}h_N^2},$$
$$\bar{D}^*_{ij}=\frac{D^*_{ij}}{A_{11N}h_N^2},\bar{F}^*_{11N}=\frac{F^*_{11N}}{A_{11N}h_N},$$
$$\bar{F}^*_{11p}=\frac{F^*_{11p}}{A_{11N}h_N},\bar{E}^*_{11N}=\frac{E^*_{11N}}{A_{11N}h_N^2},$$
$$\bar{E}^*_{11p}=\frac{E^*_{11p}}{A_{11N}h_N^2},\bar{J}^*_{11N}=\frac{J^*_{11N}}{\rho_N h_N^2},$$
$$J^*_{11p}=\frac{J^*_{11p}}{\rho_N h_N^2},\bar{G}^*_{11N}=\frac{G^*_{11N}}{\rho_N h_N^3},$$
$$G^*_{11p}=\frac{G^*_{11p}}{\rho_N h_N^3},\bar{N}^*_{xp}=\frac{N^*_{xp}V_0}{A_{11N}},$$
$$\bar{N}^*_{\theta p}=\frac{N^*_{\theta p}V_0}{A_{11N}},\bar{M}^*_{xp}=\frac{M^*_{xp}V_0}{A_{11N}h_N},$$
$$\bar{M}^*_{\theta p}=\frac{M^*_{\theta p}V_0}{A_{11N}h_N},\bar{\tau}^s_0=\frac{\tau^s_0}{A_{11N}},m_0=\frac{L}{R},$$
$$m_1=\frac{L}{h_N},m_2=\frac{h_N}{R}=\frac{1}{\bar{R}},\bar{h}_p=\frac{h_p}{R},$$
$$m_3=\frac{I}{2\rho_N h_N},m_4=\frac{h_p}{h_N},$$
$$\tau=t\sqrt{\frac{A_{11N}}{2\rho_N h_N L^2}}=\Omega t,\bar{\Omega}=\frac{\omega}{\Omega},$$
$$\bar{K}_w=\frac{K_w L^2}{m_3 A_{11N}},\bar{K}_p=\frac{K_p}{m_3 A_{11N}}, \tag{39}$$
$$\bar{C}_w=\frac{C_w\Omega L^2}{m_3 A_{11N}},\bar{\rho}_f=\frac{\rho_f}{m_3\rho_N},$$
$$\bar{u}_f=\left(VCF\times V_{no-slip}\right)\sqrt{\frac{2\rho_N h_N}{A_{11N}}},$$
$$\bar{\mu}_f=\frac{\mu_f}{m_3}\sqrt{\frac{2h_N}{\rho_N A_{11N}L^2}},\bar{V}_{DC}=\frac{V_{DC}}{V_0},$$
$$\bar{V}_{AC}=\frac{V_{AC}}{V_0},\bar{V}_p=\frac{V_p}{V_0},\bar{F}_e=\frac{\pi m_1^2 V_0^2\Upsilon}{m_3 A_{11N}},$$

Respectively, dimensionless strain and kinetic energies are obtained as follows:

$$\begin{aligned}\pi=&\frac{1}{2}\int_0^L\int_0^{2\pi}\left\{\alpha_1\left(\frac{\partial\bar{u}}{\partial\xi}\right)^2+\alpha_2\left(\frac{\partial\bar{u}}{\partial\theta}\right)^2\right.\\
&+\alpha_3\frac{\partial\bar{u}}{\partial\xi}\frac{\partial\bar{v}}{\partial\theta}+\alpha_4\frac{\partial\bar{v}}{\partial\xi}\frac{\partial\bar{u}}{\partial\theta}+\alpha_5\bar{w}\frac{\partial\bar{u}}{\partial\xi}\\
&+\alpha_6\frac{\partial\bar{u}}{\partial\xi}\left(\frac{\partial\bar{w}}{\partial\xi}\right)^2+\alpha_7\frac{\partial\bar{u}}{\partial\xi}\left(\frac{\partial\bar{w}}{\partial\theta}\right)^2\\
&+\alpha_8\frac{\partial\bar{u}}{\partial\theta}\frac{\partial\bar{w}}{\partial\xi}\frac{\partial\bar{w}}{\partial\theta}+\alpha_9\left(\frac{\partial\bar{v}}{\partial\theta}\right)^2+\alpha_{10}\frac{\partial\bar{v}}{\partial\theta}\left(\frac{\partial\bar{w}}{\partial\theta}\right)^2\\
&+\alpha_{11}\frac{\partial\bar{v}}{\partial\theta}\left(\frac{\partial\bar{w}}{\partial\xi}\right)^2+\alpha_{12}\bar{w}\frac{\partial\bar{v}}{\partial\theta}\\
&+\alpha_{13}\left(\frac{\partial\bar{v}}{\partial\xi}\right)^2+\alpha_{14}\frac{\partial\bar{v}}{\partial\xi}\frac{\partial\bar{w}}{\partial\xi}\frac{\partial\bar{w}}{\partial\theta}+\alpha_{15}\bar{w}^2\\
&+\alpha_{16}\left(\frac{\partial\bar{w}}{\partial\xi}\right)^4+\alpha_{17}\left(\frac{\partial\bar{w}}{\partial\theta}\right)^4\\
&+\alpha_{18}\left(\frac{\partial\bar{w}}{\partial\xi}\right)^2\left(\frac{\partial\bar{w}}{\partial\theta}\right)^2+\alpha_{19}\bar{w}\left(\frac{\partial\bar{w}}{\partial\xi}\right)^2\\
&+\alpha_{20}\bar{w}\left(\frac{\partial\bar{w}}{\partial\theta}\right)^2+\alpha_{21}\frac{\partial\bar{u}}{\partial\theta}\frac{\partial^2\bar{w}}{\partial\xi\partial\theta}+\alpha_{22}\frac{\partial\bar{u}}{\partial\xi}\frac{\partial^2\bar{w}}{\partial\theta^2}\\
&+\alpha_{23}\frac{\partial\bar{u}}{\partial\xi}\frac{\partial^2\bar{w}}{\partial\xi^2}+\alpha_{24}\frac{\partial\bar{v}}{\partial\theta}\frac{\partial^2\bar{w}}{\partial\xi^2}\\
&+\alpha_{25}\frac{\partial\bar{v}}{\partial\xi}\frac{\partial^2\bar{w}}{\partial\xi\partial\theta}+\alpha_{26}\frac{\partial\bar{v}}{\partial\theta}\frac{\partial^2\bar{w}}{\partial\theta^2}\\
&+\alpha_{27}\frac{\partial^2\bar{w}}{\partial\xi^2}\left(\frac{\partial\bar{w}}{\partial\theta}\right)^2+\alpha_{28}\bar{w}\frac{\partial^2\bar{w}}{\partial\xi^2}\\
&+\alpha_{29}\frac{\partial^2\bar{w}}{\partial\theta^2}\left(\frac{\partial\bar{w}}{\partial\xi}\right)^2+\alpha_{30}\frac{\partial^2\bar{w}}{\partial\xi^2}\left(\frac{\partial\bar{w}}{\partial\xi}\right)^2\\
&+\alpha_{31}\frac{\partial^2\bar{w}}{\partial\theta^2}\left(\frac{\partial\bar{w}}{\partial\theta}\right)^2+\alpha_{32}\frac{\partial^2\bar{w}}{\partial\xi\partial\theta}\frac{\partial\bar{w}}{\partial\xi}\frac{\partial\bar{w}}{\partial\theta}\\
&+\alpha_{33}\bar{w}\frac{\partial^2\bar{w}}{\partial\theta^2}+\alpha_{34}\left(\frac{\partial^2\bar{w}}{\partial\xi^2}\right)^2+\alpha_{35}\left(\frac{\partial^2\bar{w}}{\partial\theta^2}\right)^2\\
&+\alpha_{36}\left(\frac{\partial^2\bar{w}}{\partial\xi\partial\theta}\right)^2+\alpha_{37}\frac{\partial^2\bar{w}}{\partial\xi^2}\frac{\partial^2\bar{w}}{\partial\theta^2}+\alpha_{38}\bar{w}\\
&\left.+\alpha_{39}\frac{\partial\bar{u}}{\partial\xi}+\alpha_{40}\frac{\partial\bar{v}}{\partial\theta}+\alpha_{41}\left(\frac{\partial\bar{w}}{\partial\xi}\right)^2\right.\end{aligned} \tag{40}$$

$$+\alpha_{42}\left(\frac{\partial\bar{w}}{\partial\theta}\right)^2+\alpha_{43}\frac{\partial^2\bar{w}}{\partial\xi^2}+\alpha_{44}\frac{\partial^2\bar{w}}{\partial\theta^2}$$
$$+\alpha_{45}\frac{\partial^2\bar{w}}{\partial\xi^2}\frac{\partial^2\bar{w}}{\partial\tau^2}+\alpha_{46}\frac{\partial^2\bar{w}}{\partial\theta^2}\frac{\partial^2\bar{w}}{\partial\tau^2}$$
$$+\alpha_{47}\frac{\partial\bar{u}}{\partial\xi}\frac{\partial^2\bar{w}}{\partial\tau^2}+\alpha_{48}\frac{\partial\bar{v}}{\partial\theta}\frac{\partial^2\bar{w}}{\partial\tau^2}+\alpha_{49}\bar{w}\frac{\partial^2\bar{w}}{\partial\tau^2}$$
$$+\alpha_{50}\left(\frac{\partial\bar{w}}{\partial\xi}\right)^2\frac{\partial^2\bar{w}}{\partial\tau^2}+\alpha_{51}\left(\frac{\partial\bar{w}}{\partial\theta}\right)^2\frac{\partial^2\bar{w}}{\partial\tau^2}$$
$$+\eta_{33}\bar{E}_{zp}^2h_p\Big\}Rd\theta dx,$$

$$T=\frac{1}{2}\int_0^L\int_0^{2\pi}\begin{pmatrix}\left(\frac{\partial\bar{u}}{\partial\tau}\right)^2+\left(\frac{\partial\bar{v}}{\partial\tau}\right)^2\\+\left(\frac{\partial\bar{w}}{\partial\tau}\right)^2\end{pmatrix}Rd\theta dx \qquad (41)$$

where coefficients of $\alpha_k(k=1..51)$ are introduced in Appendix B.

Also, dimensionless work done by viscoelastic medium, potential due to external electric voltage, visco-pasternak effect and harmonic force, respectively, obtained as follows:

$$W_{vm}=$$
$$-\int_0^L\int_0^{2\pi}\left\{\begin{pmatrix}\bar{K}_w\bar{w}-\bar{K}_p\times\\\begin{pmatrix}\frac{\partial^2\bar{w}}{\partial\xi^2}\\+m_0^2\frac{\partial^2\bar{w}}{\partial\theta^2}\end{pmatrix}\\+\bar{C}_w\left(\frac{\partial\bar{w}}{\partial\tau}\right)\end{pmatrix}\bar{w}\right\}d\theta d\xi \qquad (42a)$$

$$W_f=$$
$$\int_0^L\int_0^{2\pi}\left\{-\begin{pmatrix}\bar{\rho}_f\frac{\partial^2\bar{w}}{\partial\tau^2}\\+2\bar{\rho}_f\bar{u}_f\frac{\partial^2\bar{w}}{\partial\xi\partial\tau}\\+\bar{\rho}_f\bar{u}_f^2\frac{\partial^2\bar{w}}{\partial\xi^2}\end{pmatrix}\right.$$
$$+\bar{\mu}_f\frac{\partial^3\bar{w}}{\partial\xi^2\partial\tau}$$
$$+m_0^2\bar{\mu}_f\frac{\partial^3\bar{w}}{\partial\theta^2\partial\tau}$$
$$+\bar{\mu}_f\bar{u}_f\frac{\partial^3\bar{w}}{\partial\xi^3}$$
$$\left.+m_0^2\bar{\mu}_f\bar{u}_f\frac{\partial^3\bar{w}}{\partial\xi\partial\theta^2}\right\}\bar{w}\,d\theta d\xi \qquad (42b)$$

$$W_e=$$
$$\int_0^L\int_0^{2\pi}\left\{\begin{pmatrix}\frac{\bar{F}_e\left(\bar{V}_{DC}\\+\bar{V}_{AC}\cos(\bar{\omega}\tau)\right)^2\bar{w}}{\sqrt{\left(\bar{b}-\bar{w}\right)\left(2\bar{R}+\bar{b}\\-\bar{w}\right)}\times}\\\left[\cosh^{-1}\left(1+\frac{\bar{b}-\bar{w}}{\bar{R}}\right)\right]^2\end{pmatrix}\right\}d\theta d\xi \qquad (42c)$$

Using electrostatic force in according to Eq. (42c), complicate solution of the obtained equation of motion. Hence it is necessary to express it to the polynomial form. For this purpose, Taylor expansion or curve fitting methods can be used. For curve fitting method, the nonlinear electrostatic force is approximated with polynomial with desired order. This is a standard problem in optimization theory and can be implemented in different mathematical software such as Matlab, Maple and Mathematica. For example lsqcurvefit function in Matlab which solve nonlinear curve-fitting (data-fitting) problems in least-squares sense can be used here. Hence with expressing the electrostatic force as a polynomial form, the dimensionless work done by electrostatic force can be express as follows:

$$W_e=$$
$$\int_0^L\int_0^{2\pi}\left\{\begin{pmatrix}\bar{F}_e\left(\bar{V}_{DC}+\\\bar{V}_{AC}\cos(\bar{\omega}\tau)\right)^2\times\\\begin{pmatrix}\bar{C}_1\\+\bar{C}_2\bar{w}+\bar{C}_3\bar{w}^2\\+\cdots+\bar{C}_n\bar{w}^{n-1}\end{pmatrix}\bar{w}\end{pmatrix}\right\}Rd\theta dx \qquad (43)$$

which $\bar{C}_1-\bar{C}_n$ are constant.

5 Solution procedure

In this section, first, discretizing equations of motion is expressed by applying the assumed mode method and then the complexification-averaging method is applied for studying of the steady state response of the system.

5.1 Discretizing equations of motion

In this section, by applying the assumed mode method, the in-plane, transverse and shear deformations can be expressed as general coordinates and mode shape functions that satisfy the geometric boundary conditions, as follows [33]:

$$\begin{bmatrix}u(x,\theta,t)\\v(x,\theta,t)\\w(x,\theta,t)\end{bmatrix}= \qquad (44)$$

$$\sum_{m=1}^{M_1}\sum_{j=1}^{N}\left[\begin{bmatrix} u_{m,j,c}(\tau)\cos(j\theta) \\ +u_{m,j,s}(\tau)\sin(j\theta)\end{bmatrix}\chi_{mj}(\xi)\right]\left[\begin{bmatrix} v_{m,j,c}(\tau)\sin(j\theta) \\ +v_{m,j,s}(\tau)\cos(j\theta)\end{bmatrix}\phi_{mj}(\xi)\right]\left[\begin{bmatrix} w_{m,j,c}(\tau)\cos(j\theta) \\ +w_{m,j,s}(\tau)\sin(j\theta)\end{bmatrix}\beta_{mj}(\xi)\right]$$
$$+\sum_{m=1}^{M_2}\begin{bmatrix} u_{m,0}(\tau)\chi_{m0}(\xi) \\ v_{m,0}(\tau)\phi_{m0}(\xi) \\ w_{m,0}(\tau)\beta_{m0}(\xi)\end{bmatrix}=$$
$$\sum_{(i,r,s)=1}^{M_2+M_1\times N}\begin{bmatrix} u_i(\tau)\chi_i(\xi)\vartheta_i(\theta) \\ v_r(\tau)\phi_r(\xi)\alpha_r(\theta) \\ w_s(\tau)\beta_s(\xi)\psi_s(\theta)\end{bmatrix},$$

where $\chi_i(\xi)$, $\phi_r(\xi)$ and $\beta_s(\xi)$ are modal functions which satisfy the required geometric boundary conditions. $u_i(\tau)$, $v_r(\tau)$ and $w_s(\tau)$ are unknown functions of time and are related to dynamical response.

Substituting Eqs. (44) into Eqs. (40)- (43) and applying the Lagrange eqtions:

$$\frac{\partial}{\partial\tau}\left(\frac{\partial T}{\partial\dot{\bar{q}}_i}\right)-\left(\frac{\partial T}{\partial\bar{q}_i}\right)+\left(\frac{\partial\pi}{\partial\bar{q}_i}\right)=\sum\left(\frac{\partial W}{\partial\bar{q}_i}\right),\quad(\bar{q}=\bar{u},\bar{v},\bar{w}\,) \tag{45}$$

Where $W=W_{vm}+W_f+W_e$.

Results in the following reduced-order model of the system:

$$[(M)_u^u]\{\ddot{\bar{u}}\}+[(M)_u^w]\{\ddot{\bar{w}}\}+[(K)_u^u]\{\bar{u}\}+[(K)_u^v]\{\bar{v}\}+[(K)_u^w]\{\bar{w}\}+[(NL)_u^w]\{\bar{w}^2\}=\left[\bar{F}_{up}\right], \tag{46}$$

$$[(M)_v^v]\{\ddot{\bar{v}}\}+[(M)_v^w]\{\ddot{\bar{w}}\}+[(K)_v^u]\{\bar{u}\}+[(K)_v^v]\{\bar{v}\}+[(K)_v^w]\{\bar{w}\}+[(NL)_v^w]\{\bar{w}^2\}=\left[\bar{F}_{vp}\right], \tag{47}$$

$$\left[(M)_w^w+(K)_{w2}^{\ddot{w}}\{\bar{w}\}\right]\{\ddot{\bar{w}}\}+[(c)_w^w]\{\dot{\bar{w}}\}+[(K)_w^u]\{\bar{u}\}+[(K)_w^v]\{\bar{v}\}+[(K)_w^w]\{\bar{w}\}+[(NL)_w^u]\{\bar{w}\bar{u}\}+[(NL)_w^v]\{\bar{w}\bar{v}\}+[(NL)_{w2}^w]\{\bar{w}^2\}+[(NL)_{w3}^w]\{\bar{w}^3\}=[\bar{F}_{we}]+\left[\bar{F}_{wp}\right]+\left[\bar{F}_e\begin{Bmatrix}(\bar{V}_{AC}cos\bar{\omega}\tau)^2\\ +2\bar{V}_{AC}\bar{V}_{DC}cos\bar{\omega}\tau\end{Bmatrix}\times\begin{Bmatrix}\bar{C}_4(NL_{3e})_w^w+\bar{C}_3(NL_{2e})_w^w\\ +\bar{C}_2(K_e)_w^w+\bar{C}_1\bar{F}_1\end{Bmatrix}\right], \tag{48}$$

where $(M),(C)$ and (K) are mass, damping and linear stiffness matrixes. $(NL)_u^w,(NL)_v^w$, and $(NL)_{w2}^w$ are second-order nonlinear stiffness matrixes and $(NL)_{w3}^w$ is third-order nonlinear stiffness matrix. Also, K_e, NL_{2e} and NL_{3e} are the linear stiffness, second and third order nonlinear stiffness matrixes for electrostatic force expansion, respectively. Also, $\bar{F}_{up}$, $\bar{F}_{vp}$ and $\bar{F}_{wp}$ are applied loads by piezoelectric voltage and surface stress. All coefficients of mass, stiffness, linear and nonlinear term matrixes and applied loads Eqs. (46) - (48) are presented in Appendix C.

Natural frequencies and mode shapes can be obtained from solving following eigenvalue equation:

$$\left[[K]+i\omega_{mn}[C]-\omega_{mn}^2[M]\right]\times\{u_{mn}\ \ v_{mn}\ \ w_{mn}\}^T=0, \tag{49}$$

6 Results and Discussions

In this section, first, comparing the present numerical results of macroscopic cylindrical shell with previously published in the literature is presented for arbitrary boundary conditions and convergence study of a Piezoelectric biomedical nanosensor (PBMNS) based on nano-shell with simply supported boundary condition is investigated for Gurtin–Murdoch surface/interface theory. Then estimation of the natural frequency, critical fluid velocity and stability analysis of piezoelectric biomedical nanosensor conveying viscous bloodstream is investigated using the electro-elastic Gurtin–Murdoch surface/interface theory and considering von-karman-Donnell's shell model. In order to simplify the presentation, CC, SS, CS and CF represent clamped edges, simply supported edges, clamped-simply supported edges and clamped-free edges, respectively and also for simplification of surface effect is represented SE. The material properties for nonhomogeneous nano-shell and piezoelectric layer are shown in Table 1-2, respectively [42].

Table 1. Properties of stainless steel and nickel [42]

Stainless steel			Nichel		
$E_B(GPa)$	υ_B	$\rho_B(kg\,m^{-3}$	$E_T(GPa)$	υ_T	$\rho_T(kg\,m^{-3}$
208	0.381	8166	205	0.31	8900

Table 2. Properties of PZT-4 [42]

$E_p(GP$	υ_p	$e_{31p}(C/n$	$e_{32p}(C/n$	$\eta_{33p}(10^{-11}$ F	$\rho_p(kg\,m$
95	0.3	−5.2	−5.2	560	7500

The material and geometrical parameters used in all following results are shown in Table 3.

Table 3. The material and geometrical parameters [20, 37, 43-44]

$R(m)$	L/R	h_N/R	h_p/R	$\lambda^{S_1}(N/n$	$\mu^{S_1}(N/n$
$1\times10^-$	10	0.02	0.02	4.488	2.774
$\tau_0^{S_1}$ (N/m)	$\rho^{S_1}(kg/$	$V_p(V)$	$\lambda^{S_2}(N/m$	$\mu^{S_2}(N/n$	$\tau_0^{S_2}(N/n$
0.6	3.17×1	1×10^{-5}	4.488	2.774	0.6
$e_{31p}^{S_2}(C/$	$e_{32p}^{S_2}(C/$	$\rho^{S_2}(kg/$	$C_w(N.S/$	$K_w(N/n$	$K_p(N/n$

-3×10	-3×10	5.61×1	1×10^{-1}	8.99950×10^{17}	2.07127
$V_{AC}(V)$	$V_{DC}(V)$	b/R	V_0	$\mu_f(pa.s$	$\rho_f(kg/$
3	1	2	1	$3\times 10^{-}$	1060

Of course, the geometrical parameters can be varying according to the type of problem. In this paper, the results are presented in dimensionless form and thus the results are not limited to a particular type of matter. The data presented in the form of sample data to approximate the numbers used in the actual range.

6.1 Convergence and comparison studies

The method proposed in this paper is validated by comparing the present numerical results with previously published in the literature. If we neglect the piezoelectric, visco-Pasternak and surface effects, the present model can be reduced to the macroscopic cylindrical shell model. The dimensionless natural frequencies $\left(\omega_n = \Omega R\sqrt{(1-\upsilon^2)\rho/E}\right)$ of present work are compared with macroscopic cylindrical shell which previously given by Loy et al. [29] that is shown in Table 4 for the three classical boundary conditions. The parameters used in this example are: $m = 1$, $L/R = 20$, $h_N/R = 0.01$, and $\upsilon = 0.3$. It can be observed from Table 5 that the present results agree very well with the reference solutions, which indicates that the method presented in this paper is suitable and of high accuracy for free vibration analysis of cylindrical shells with classical boundary conditions. The slight differences in the results may be attributed to the different shell theories and solution approaches adopted in the literature and in this paper.

Table 4. Comparison of dimensionless natural frequencies $\left(\omega_n = \Omega R\sqrt{(1-\upsilon^2)\rho/E}\right)$ for SS, SC and CC boundary conditions for a homogeneous cylindrical shells with $m = 1$, $L/R = 20$, $h_N/R = 0.01$, and $\upsilon = 0.3$.

n	SS		CS		CC	
	Present	Loy [29]	Present	Loy [29]	Present	Loy [29]
1	0.016101	0.016101	0.023299	0.023974	0.032074	0.032885
2	0.009235	0.009382	0.010963	0.011225	0.013202	0.013932
3	0.021753	0.022105	0.020953	0.022310	0.019713	0.022672
4	0.039307	0.042095	0.041300	0.042139	0.041386	0.042208

Complete convergence for the dimensionless natural frequencies $\bar{\Omega}_n$ and dimensionless damping frequencies $\bar{\Omega}_d$ of SS piezoelectric biomedical nanosensor considering with the Gurtin–Murdoch surface/interface theory and the material and geometrical parameters of Tables (1-3) is shown in Tables 5 and 6, respectively.

Table 5. Convergence of dimensionless natural frequencies $\bar{\Omega}_n$ of the SS piezo piezoelectric elastic biomedical nanosensor

n	$N=1$	$N=2$	$N=3$	$N=5$
2	0.8107340 4357	0.8107351 0782	0.8107351 0781	0.8107351 6796
3	1.8151243 0896	1.8151572 0073	1.8151571 8273	1.8151580 8628
4	2.8327282 9570	2.8328471 2539	2.8328467 7062	2.8328504 1730

Table 6. Convergence of dimensionless damp frequencies $\bar{\Omega}_d$ of the SS piezoelectric biomedical nanosensor

n	$N=1$	$N=2$	$N=3$	$N=5$
2	0.8062114 8043	0.8062124 2314	0.8062124 2313	0.8062124 7871
3	1.8029349 1873	1.8029658 5533	1.8029658 4049	1.8029666 9801
4	2.8103357 1036	2.8104503 3736	2.8104500 1216	2.8104535 3764

It is observed that the number of polynomial terms, N, is increased, the value of the frequency parameter $(\bar{\Omega}_n, \bar{\Omega}_d)$, converges rapidly. With considering of the two succesasing values of N, it is shows that as N increases, the percentage difference between the successive frequency approximations decreases. Thus the error as shown above is less 1 per cent, which is well within the limits of engineering tolerance. The minimum frequency in this case is associated with the circumferential wave number $n = 2$. This assertion is valid for the entire range of shell.

6.2 Parametric study

The convergence and comparison study of the present work was verified in the previous subsection. In this subsection, dimensionless frequencies $\bar{\Omega}$ versus dimensionless fluid (bloodstream) velocity $\bar{u}_f$ for stability analysis and estimation of critical fluid velocity of a SS piezoelectric biomedical nanosensor (PBMNS) are presented in Figures 2-10 with respect to the different geometrical and material parameters such

as the ratio of the length of the nanosystem to the radius L/R, the ratio of nanoshell thickness to radius h_N/R, the ratio of the piezoelectric thickness to the radius h_p/R, the effects of the viscoelastic medium ($\bar{K}_w$, $\bar{K}_p$, $\bar{C}_w$), the piezoelectric voltage V_p and also surface energy effects. As shown in these figures, the frequency is decreased as the flow velocity is increased.

Figure 2 demonstrate in the dimensionless frequency ($\bar{\Omega}$) versus fluid velocity ($\bar{u}_f$) for the first five vibration modes of the PBMNS. It can be seen that $\bar{\Omega}_n$ reduces with increased $\bar{u}_f$. For zero natural frequency, PBMNS becomes unstable and the corresponding fluid velocity is called the critical flow velocity. As can be seen, the critical fluid velocity correspond to the 1^{st} and 2^{nd} modes is reached at the vicinity of $\bar{u}_f \cong 6.894$. This physically implies that the DWBNNT losses its stability due to the divergence via a pitchfork bifurcation while the 3^{rd}, 4^{th} and 5^{th} modes are still stable. Thereafter, for the fluid velocity within the range $6.894 \leq \bar{u}_f \leq 7.23$, the first amd second modes are zero, which the system becomes unstable. As the flow velocity reaches about $\bar{u}_f \cong 7.23$, natural frequencies in the 1^{st} mode return to positive and the system tends to regains stability in the first mode, while, the 2^{nd} mode still remain instable. Also, the PBMNS becomes unstable at 3^{rd} mode when $\bar{u}_f \cong 7.248$. This phenomenon may be observed in different modes for higher velocities in this figure. The same behavior can also be observed for other vibration modes of following figures.

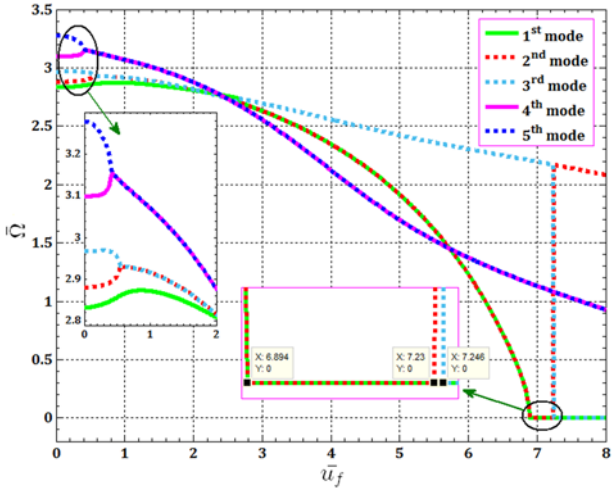

Fig. 2. Dimensionless frequencies $\bar{\Omega}$ versus fluid velocity $\bar{u}_f$ for the first five vibration modes of SS piezoelectric biomedical nanosensor

The effect of length-to-small radius ratio (L/R) on dimensionless natural $\bar{\Omega}_n$ versus dimensionless fluid velocity $\bar{u}_f$ for SS piezoelectric biomedical nanosensor is illustrated in Figure 3. It is evident that natural frequencies and critical fluid velocity of the PBMNS increase with increasing L/R. As can be seen, the critical fluid velocity corresponds to the lower value of $L/R = 5$ sooner than the rest values of this ratio are reached to be zero. This physically implies that first the PBMNS in $L/R = 5$ losses its stability due to the divergence via a pitchfork bifurcation. In addition, the length-to-small radius ratio of cylindrical shell has an important effect on natural frequency. The reason is that a higher L/R ratio leads to increase in the nanoshell stiffness, and cause to higher natural frequencies of nanoshells.

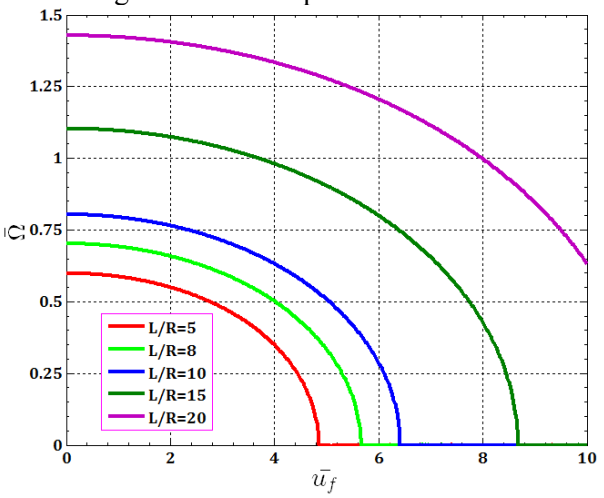

Fig. 3. The dimensionless frequencies $\bar{\Omega}$ versus fluid velocity $\bar{u}_f$ of SS piezoelectric biomedical nanosensor for different values of L/R ratio

Figure 4 illustrates the effect of thickness shell to small radius ratio h_N/R on dimensionless natural frequencies $\bar{\Omega}_n$ versus dimensionless fluid velocity $\bar{u}_f$ for SS piezoelectric biomedical nanosensor.

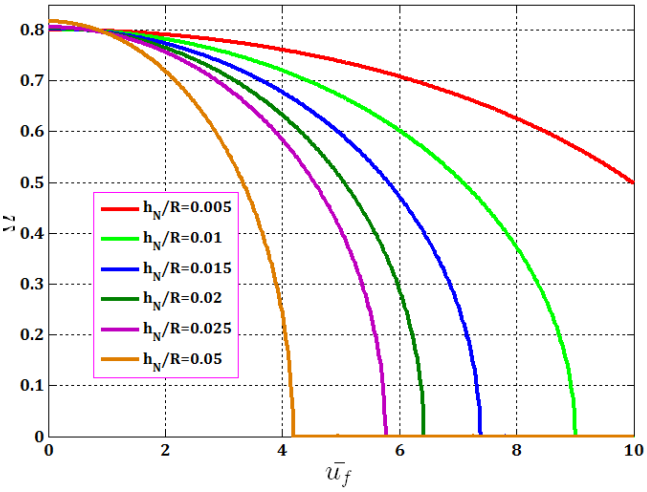

Fig. 4. The dimensionless frequencies $\bar{\Omega}$ versus fluid velocity $\bar{u}_f$ of SS piezoelectric biomedical nanosensor for different values of h_N/R ratio

It can be seen that with the increasing of the nanoshell stiffness ratio (h_N/R), the natural frequency $\bar{\Omega}$ and the critical fluid velocity $\bar{u}_f$ decrease. Also, the critical fluid velocity corresponds to the higher value of $h_N/R = 0.05$ sooner than the rest values of this ratio are reached to be zero. This physically implies that first the PBMNS in $h_N/R = 0.05$ losses its stability due to the divergence via a pitchfork bifurcation.

The effect of piezoelectric thickness to small radius ratio (h_p/R) on dimensionless natural frequencies $\bar{\Omega}_n$ versus dimensionless fluid velocity $\bar{u}_f$ is presented in Figure 5. It can be seen that unlike previous results for h_N/R ratio, in this case with the increasing of the piezoelectric thickness to small radius ratio, the natural frequency $\bar{\Omega}$ and the critical fluid velocity $\bar{u}_f$ increase. Also, the critical fluid velocity corresponds to the lower value of $h_p/R = 0.005$ sooner than the rest values of this ratio are reached to be zero. This physically implies that first the PBMNS in $h_p/R = 0.005$ losses its stability due to the divergence via a pitchfork bifurcation.

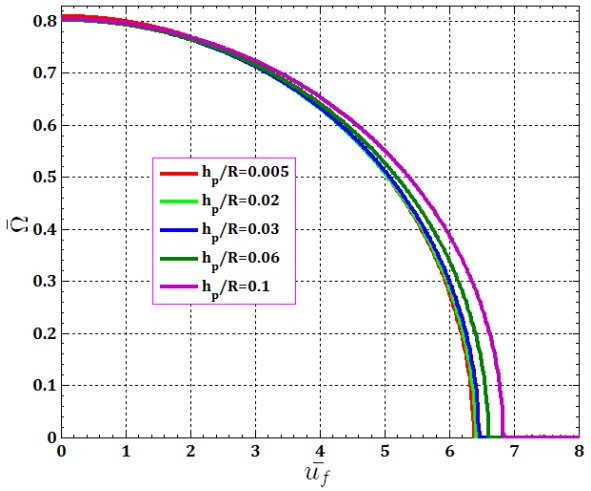

Fig. 5. The dimensionless frequencies $\bar{\Omega}$ versus fluid velocity $\bar{u}_f$ of SS piezoelectric biomedical nanosensor for different values of h_p/R ratio

Figures 6 and 7 respectively illustrate dimensionless stiffness coefficient of Winkler foundation $\bar{K}_w$ and shear layer of Pasternak foundation $\bar{K}_p$ on dimensionless natural frequencies $\bar{\Omega}_n$ versus dimensionless fluid velocity $\bar{u}_f$ for SS piezoelectric biomedical nanosensor. In both case, it can be seen that with the increasing of $\bar{K}_w$ and $\bar{K}_p$ ratios, the natural frequency $\bar{\Omega}$ and the critical fluid velocity $\bar{u}_f$ increase.

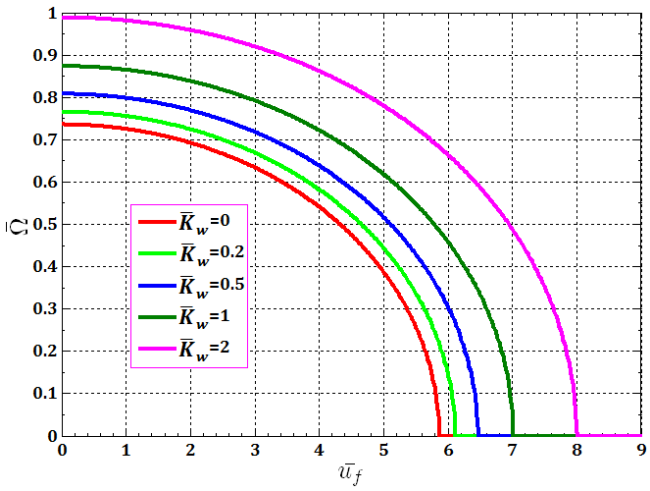

Fig. 6. The dimensionless frequencies $\bar{\Omega}$ versus fluid velocity $\bar{u}_f$ of SS piezoelectric biomedical nanosensor for different values of $\bar{K}_w$

This is perhaps because increasing Winkler and Pasternak coefficients increases the shell stiffness. For zero natural frequency, PBMNS becomes unstable and this physically implies that the PBMNS losses its stability due to the divergence via a pitchfork bifurcation.

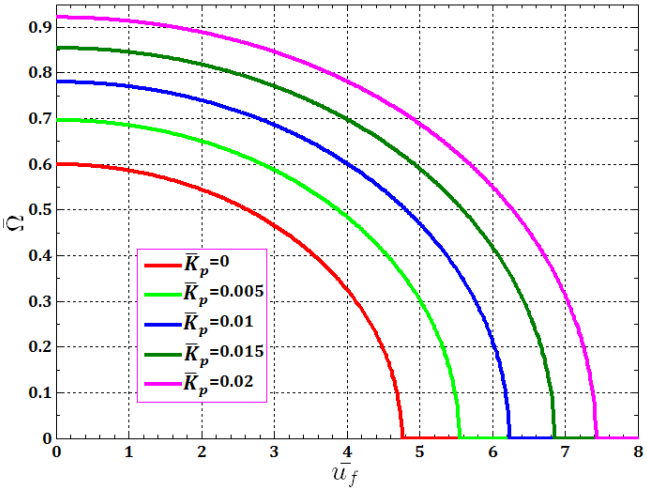

Fig. 7. The dimensionless frequencies $\bar{\Omega}$ versus fluid velocity $\bar{u}_f$ of SS piezoelectric biomedical nanosensor for different values of $\bar{K}_p$

Figure 8 presents the effect of dimensionless damping coefficient $\bar{C}_w$ on dimensionless damp frequencies $\bar{\Omega}_d$ versus dimensionless fluid velocity $\bar{u}_f$ for SS piezoelectric biomedical nanosensor. It can be seen that with the increasing of damper coefficient, the natural frequency $\bar{\Omega}$ and the critical fluid velocity $\bar{u}_f$ decrease. Also, the critical fluid velocity corresponds to the higher value of $\bar{C}_w$ sooner than the rest values of this ratio are reached

to be zero and system losses its stability due to the divergence via a pitchfork bifurcation.

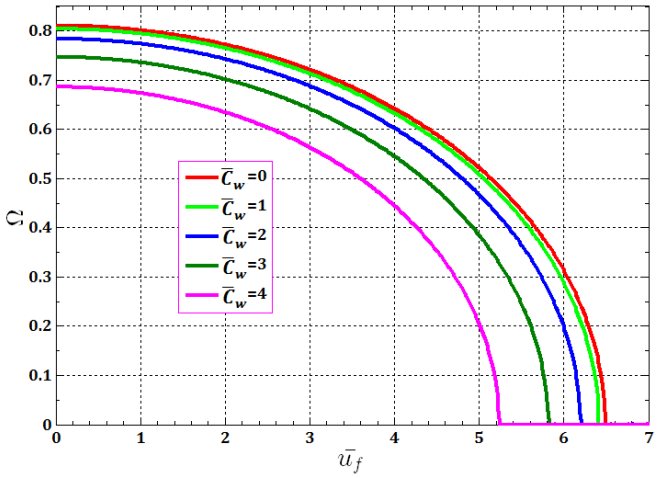

Fig. 8. The dimensionless frequencies $\bar{\Omega}$ versus fluid velocity $\bar{u}_f$ of SS piezoelectric biomedical nanosensor for different values of $\bar{C}_w$

Figure 9 presents the effect of several of surrounding medium on dimensionless natural frequencies $\bar{\Omega}_n$ with respect to the dimensionless fluid velocity $\bar{u}_f$. As can be seen, without medium, Winkler ($\bar{K}_w$), Pasternak ($\bar{K}_p$), visco ($\bar{C}_w$), visco-Winkler ($\bar{K}_w + \bar{C}_w$), visco- Pasternak ($\bar{K}_p + \bar{C}_w$), Winkler-Pasternak ($\bar{K}_w + \bar{K}_p$) and Visco-medium ($\bar{K}_w + \bar{K}_p + \bar{C}_w$), are eight assumptions medium in this work. It can be founded, that the frequency and the critical velocity have minimum and maximum values when the system respectively has with and without damping coefficient. In this results indicate that the system tends to be very sensitive to whether or not there is a damping coefficient in all cases. Also, it is worth mentioning that critical velocity in Pasternak foundation is more than critical velocity predicted by Winkler foundation. This is due to the fact that the Winkler foundation describes the effect of the normal stress of the elastic medium, whereas Pasternak elastic foundation describes the effect of the tangential and normal stresses of the elastic medium.

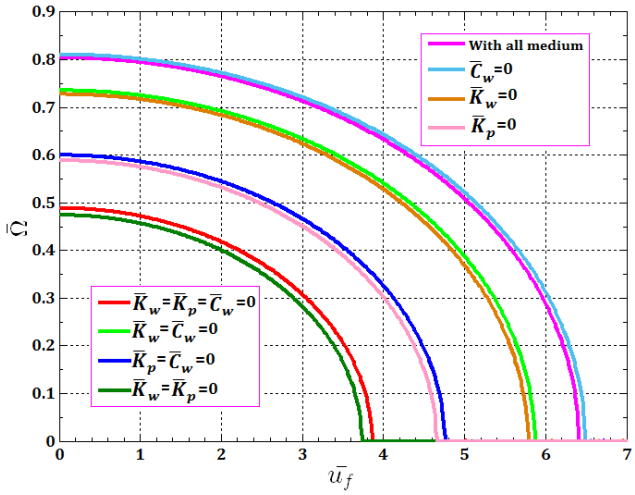

Fig. 9. The dimensionless frequencies $\bar{\Omega}$ versus fluid velocity $\bar{u}_f$ of SS piezoelectric biomedical nanosensor for different cases of Visco-medium

The effect of piezoelectric voltage V_p on dimensionless natural frequencies $\bar{\Omega}_n$ versus dimensionless fluid velocity $\bar{u}_f$ for SS piezoelectric biomedical nanosensor is illustrated in Figure 10.

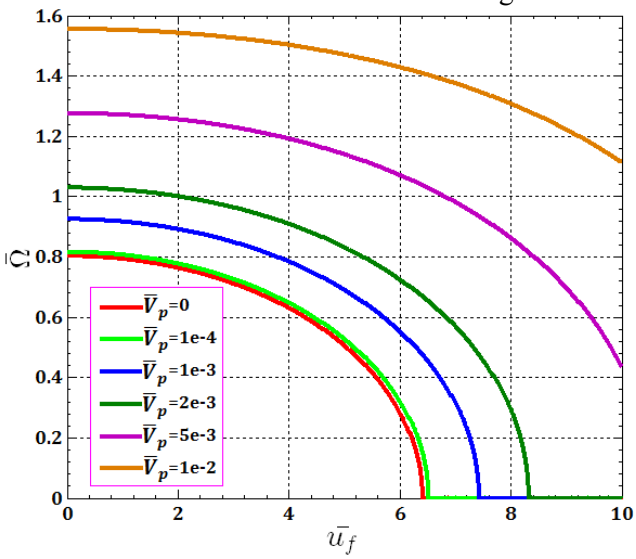

Fig. 10. The dimensionless frequencies $\bar{\Omega}$ versus fluid velocity $\bar{u}_f$ of SS piezoelectric biomedical nanosensor for different values of $\bar{V}_p$

As shown in this Figure, with the increasing of $\bar{V}_p$, the natural frequency $\bar{\Omega}$ and the critical fluid velocity $\bar{u}_f$ increase. This is perhaps because increasing piezoelectric voltage increases the nanoshell stiffness. For zero natural frequency, PBMNS becomes unstable and this physically implies that the PBMNS losses its stability due to the divergence via a pitchfork bifurcation.

And in end, dimensionless natural frequencies $\bar{\Omega}_n$ versus dimensionless fluid velocity $\bar{u}_f$ for SS piezoelectric biomedical nanosensor with and

without surface energy effects are shown in Figures 11. As show in results, the most important parameters on natural frequencies and fluid velocity is surface density (ρ_{NI}, ρ_{PS}) that with regardless of this parameter, the critical fluid velocity sooner than the rest parameters are reached to be zero and system losses its stability due to the divergence via a pitchfork bifurcation but in this case system has maximum natural frequency due to higher stiffness of nanoshell in this case. Also when all surface effect is considered, the critical fluid velocity later than the rest parameters are reached to be zero.

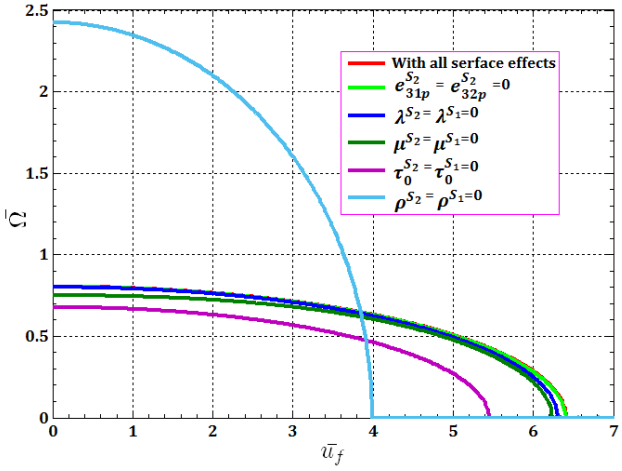

Fig. 11. Surface energy effects on the dimensionless frequencies $\bar{\Omega}$ versus fluid velocity $\bar{u}_f$ of SS piezoelectric biomedical nanosensor

7 Conclusion

In current study, the natural frequency, critical fluid velocity and stability analysis of piezoelectric biomedical nanosensor (PBMNS) based on cylindrical nanoshell conveying viscous fluid is investigated using the electro-elastic Gurtin–Murdoch surface/interface theory, Hamilton's principle and also the assumed mode method combined with Euler – Lagrange. This system subjected to nonlinear electrostatic field, viscoelastic medium including visco-pasternak and damping coefficients. The convergence, accuracy and reliability of the current formulation are validated by comparisons with existing results. Also stability analysis and dimensionless natural frequency versus dimensionless fluid velocity of a piezoelectric biomedical nanosensor are accurately studied with respect to the different geometrical and material parameters.

Some conclusions are obtained from this study:

- ✓ With comparing the previously published in the literature, the present results agree very well with the reference solutions, which indicates that the methods are suitable and of high accuracy for free vibration analysis of cylindrical nanoshell.
- ✓ In convergence study, as the number of polynominal terms, N, is increased, the value of the frequency parameter, $\bar{\Omega}_n$, converges rapidly and also the convergence mode number is $m = 2$ and $n = 2$ and this means that two longitudinal mode and in according to Eq. (45), five peripheral modes, and totally fifteen number of mode shapes can represent the response of system with sufficient degrees.
- ✓ In the 1^{st} and 2^{nd} modes, at the vicinity of the critical flow velocity 6.894, natural frequency equal to zero, where divergence instability occurs due to pitchfork bifurcation while at this critical flow velocity, the 3^{rd}, 4^{th} and 5^{th} modes still remain stable.
- ✓ As the flow velocity reaches about 7.23 , natural frequencies in the 1^{st} mode return to positive and the system tends to regains stability in the first mode, while, the 2^{nd} mode still remain instable. The same behavior can also be observed for other vibration modes.
- ✓ For all following results, zero natural frequency of PBMNS becomes unstable and this physically implies that the PBMNS losses its stability due to the divergence via a pitchfork bifurcation.
- ✓ Natural frequencies and critical fluid velocity increase with increasing of L/R, h_p/R, $\bar{K}_w$, $\bar{K}_p$ and $\bar{V}_p$ and the critical fluid velocity corresponds to the lower value sooner than the rest values of this ratio are reached to be zero. This is perhaps because increasing Winkler and Pasternak coefficients increases the shell stiffness.
- ✓ with the increasing of damper coefficient and h_p/R ratio the natural frequency $\bar{\Omega}$ and the critical fluid velocity $\bar{u}_f$ decrease.
- ✓ the frequency and the critical velocity have minimum and maximum values when the system respectively has with and without damping coefficient. In this results indicate that the system tends to be very sensitive to whether or not there is a damping coefficient in all cases.
- ✓ the most important parameters on natural frequencies and fluid velocity is surface density (ρ_{NI}, ρ_{PS}) that with regardless of this parameter, the critical fluid velocity sooner than the rest parameters are reached to be zero but in this case system has maximum natural frequency due to higher stiffness of nanoshell in this case.

- ✓ when all surface effect is considered, the critical fluid velocity later than the rest parameters are reached to be zero.

Conflict of interest

The authors report no conflict of interest.

Funding Acknowledgement

'This research received no specific grant from any funding agency in the public, commercial, or not-for-profit sectors'.

Appendix A

The stresses and moment resultants:

$$(N_{xx}, N_{\theta\theta}, N_{x\theta}) = \int_{-h_N}^{h_N} \sigma_{ijN}\, dz + \int_{h_N}^{h_N+h_p} \sigma_{ijp}\, dz + \sigma_{s_1} + \sigma_{s_2} = (N_{xN}, N_{\theta N}, N_{x\theta N}) + (N_{xp}, N_{\theta p}, N_{x\theta p}) + \left(\sigma_{xx}, \sigma_{\theta\theta}, \frac{1}{2}(\sigma_{x\theta} + \sigma_{\theta x})\right)_{s_1} + \left(\sigma_{xx}, \sigma_{\theta\theta}, \frac{1}{2}(\sigma_{x\theta} + \sigma_{\theta x})\right)_{s_2} \quad (A.1)$$

$$(M_{xx}, M_{\theta\theta}, M_{x\theta}) = \int_{-h_N}^{h_N} \sigma_{ijN}\, z dz + \int_{h_N}^{h_N+h_p} \sigma_{ijp}\, z dz + \sigma_{s_2}(h_N + h_p) - \sigma_{s_1} h_N = (M_{xN}, M_{\theta N}, M_{x\theta N}) + (M_{xp}, M_{\theta p}, M_{x\theta p}) + \left(\sigma_{xx}, \sigma_{\theta\theta}, \frac{1}{2}(\sigma_{x\theta} + \sigma_{\theta x})\right)_{s_2} (h_N + h_p) - \left(\sigma_{xx}, \sigma_{\theta\theta}, \frac{1}{2}(\sigma_{x\theta} + \sigma_{\theta x})\right)_{s_1} h_N \quad (A.2)$$

$$N_{xx} = A_{11}\varepsilon_{xx}^0 + A_{12}\varepsilon_{\theta\theta}^0 + B_{11}\kappa_{xx} + B_{12}\kappa_{\theta\theta} - \frac{1}{2}(\tau_0^{s_1} + \tau_0^{s_2})\left(\frac{\partial w}{\partial x}\right)^2 + (\tau_0^{s_1} + \tau_0^{s_2} - N_{xp}) + F_{11}^*\left(\frac{\partial^2 w}{\partial x^2} + \frac{1}{R^2}\frac{\partial^2 w}{\partial \theta^2}\right) + J_{11}^*\frac{\partial^2 w}{\partial t^2}, \quad (A.3)$$

$$N_{\theta\theta} = A_{21}\varepsilon_{xx}^0 + A_{22}\varepsilon_{\theta\theta}^0 + B_{21}\kappa_{xx} + B_{22}\kappa_{\theta\theta} - \frac{1}{2}(\tau_0^{s_1} + \tau_0^{s_2})(\frac{2w}{R} + \frac{1}{R^2}(\frac{\partial w}{\partial \theta})^2) + (\tau_0^{s_1} + \tau_0^{s_2} - N_{\theta p}) + F_{11}^*\left(\frac{\partial^2 w}{\partial x^2} + \frac{1}{R^2}\frac{\partial^2 w}{\partial \theta^2}\right) + J_{11}^*\frac{\partial^2 w}{\partial t^2}, \quad (A.4)$$

$$N_{x\theta} = A_{66}\gamma_{x\theta}^0 + B_{66}\kappa_{x\theta}, \quad (A.5)$$

$$M_{xx} = B_{11}\varepsilon_{xx}^0 + B_{12}\varepsilon_{\theta\theta}^0 + D_{11}\kappa_{xx} + D_{12}\kappa_{\theta\theta} + \tau_0^{s_2}(1 - \frac{1}{2}(\frac{\partial w}{\partial x})^2)(h_N + h_p) - \tau_0^{s_1}(1 - \frac{1}{2}\left(\frac{\partial w}{\partial x}\right)^2)h_N - M_{xp} + E_{11}^*(\frac{\partial^2 w}{\partial x^2} + \frac{1}{R^2}\frac{\partial^2 w}{\partial \theta^2}) + G_{11}^*\frac{\partial^2 w}{\partial t^2}, \quad (A.6)$$

$$M_{\theta\theta} = B_{21}\varepsilon_{xx}^0 + B_{22}\varepsilon_{\theta\theta}^0 + D_{21}\kappa_{xx} + D_{22}\kappa_{\theta\theta} + \tau_0^{s_2}(1 - \frac{1}{2}(\frac{2w}{R} + \frac{1}{R^2}(\frac{\partial w}{\partial \theta})^2))(h_N + h_p) - \tau_0^{s_1}\left(1 - \frac{1}{2}\left(\frac{2w}{R} + \frac{1}{R^2}\left(\frac{\partial w}{\partial \theta}\right)^2\right)\right)h_N - M_{\theta p} + E_{11}^*(\frac{\partial^2 w}{\partial x^2} + \frac{1}{R^2}\frac{\partial^2 w}{\partial \theta^2}) + G_{11}^*\frac{\partial^2 w}{\partial t^2}, \quad (A.7)$$

$$M_{x\theta} = B_{66}\gamma_{x\theta}^0 + D_{66}\kappa_{x\theta}, \quad (A.8)$$

in which

$$A_{ij} = A_{ijN} + A_{ijp} + A_{ij}^*, \quad B_{ij} = B_{ijN} + B_{ijp} + B_{ij}^*, \quad D_{ij} = D_{ijN} + D_{ijp} + D_{ij}^*, \quad F_{11}^* = F_{11N}^* + F_{11p}^*, J_{11}^* = J_{11N}^* + J_{11p}^*, \quad E_{11}^* = E_{11N}^* + E_{11p}^*, G_{11}^* = G_{11N}^* + G_{11p}^*, \quad (A.9)$$

and

$$(A_{ijN}, B_{ijN}, D_{ijN}) = \int_{-h_N}^{h_N} C_{ijN}(1, z, z^2)\, dz, (A_{ijp}, B_{ijp}, D_{ijp}) = \int_{h_N}^{h_N+h_p} C_{ijp}(1, z, z^2)\, dz, \quad (A.10)$$

$$(N_{xp}, N_{\theta p}) = \int_{h_N}^{h_N+h_p} (e_{31p}, e_{32p})\bar{E}_{zp}\, dz + (e_{31p}^s, e_{32p}^s)\bar{E}_{zp}, \quad (A.11)$$

$$(M_{xp}, M_{\theta p}) = \int_{h_N}^{h_N+h_p} (e_{31p}, e_{32p})\bar{E}_{zp}\, z dz + (e_{31p}^s, e_{32p}^s)\bar{E}_{zp}(h_N + h_p), \quad (A.12)$$

$$A_{11}^* = A_{22}^* = (\lambda^{s_1} + 2\mu^{s_1}) + (\lambda^{s_2} + 2\mu^{s_2}), \quad A_{12}^* = A_{21}^* = (\tau_0^{s_1} + \lambda^{s_1}) + (\tau_0^{s_2} + \lambda^{s_2}), \quad A_{66}^* = (\mu^{s_1} - \frac{\tau_0^{s_1}}{2}) + (\mu^{s_2} - \frac{\tau_0^{s_2}}{2}), \quad (A.13)$$

$$B_{11}^* = B_{22}^* = (\lambda^{s_2} + 2\mu^{s_2})(h_N + h_p) - (\lambda^{s_1} + 2\mu^{s_1})(h_N), \quad B_{12}^* = B_{21}^* = (\tau_0^{s_2} + \lambda^{s_2})(h_N + h_p) - (\tau_0^{s_1} + \lambda^{s_1})(h_N), \quad (A.14)$$

$$B_{66}^{*}=(\mu^{s_2}-\frac{\tau_0^{s_2}}{2})\big(h_N+h_p\big)-(\mu^{s_1}-\frac{\tau_0^{s_1}}{2})(h_N),$$
$$D_{11}^{*}=D_{22}^{*}=(\lambda^{s_2}+2\mu^{s_2})\big(h_N+h_p\big)^2+(\lambda^{s_1}+2\mu^{s_1})(h_N)^2,$$
$$D_{12}^{*}=D_{21}^{*}=\big(\tau_0^{s_2}+\lambda^{s_2}\big)\big(h_N+h_p\big)^2+\big(\tau_0^{s_1}+\lambda^{s_1}\big)(h_N)^2,$$
$$D_{66}^{*}=(\mu^{s_2}-\frac{\tau_0^{s_2}}{2})\big(h_N+h_p\big)^2+(\mu^{s_1}-\frac{\tau_0^{s_1}}{2})(h_N)^2,$$
(A.15)

$$F_{11N}^{*}=\int_{-h_N}^{h_N}\frac{\upsilon_N}{(1-\upsilon_N)}\begin{pmatrix}\frac{(\tau_0^{s_2}-\tau_0^{s_1})}{2}\\+\frac{(\tau_0^{s_2}+\tau_0^{s_1})z}{2h_N+h_p}\end{pmatrix}dz,$$
$$F_{11p}^{*}=\int_{h_N}^{h_N+h_p}\frac{\upsilon_p}{(1-\upsilon_p)}\begin{pmatrix}\frac{(\tau_0^{s_2}-\tau_0^{s_1})}{2}\\+\frac{(\tau_0^{s_2}+\tau_0^{s_1})z}{2h_N+h_p}\end{pmatrix}dz,$$
(A.16)

$$J_{11N}^{*}=\int_{-h_N}^{h_N}\frac{\upsilon_N}{(1-\upsilon_N)}\begin{pmatrix}\frac{(\rho^{s_1}-\rho^{s_2})}{2}\\-\frac{(\rho^{s_1}+\rho^{s_2})z}{2h_N+h_p}\end{pmatrix}dz,$$
$$J_{11p}^{*}=\int_{h_N}^{h_N+h_p}\frac{\upsilon_p}{(1-\upsilon_p)}\begin{pmatrix}\frac{(\rho^{s_1}-\rho^{s_2})}{2}\\-\frac{(\rho^{s_1}+\rho^{s_2})z}{2h_N+h_p}\end{pmatrix}dz,$$
(A.17)

$$E_{11N}^{*}=\int_{-h_N}^{h_N}\frac{\upsilon_N}{(1-\upsilon_N)}\begin{pmatrix}\frac{(\tau_0^{s_2}-\tau_0^{s_1})z}{2}\\+\frac{(\tau_0^{s_2}+\tau_0^{s_1})z^2}{2h_N+h_p}\end{pmatrix}dz,$$
$$E_{11p}^{*}=\int_{h_N}^{h_N+h_p}\frac{\upsilon_p}{(1-\upsilon_p)}\begin{pmatrix}\frac{(\tau_0^{s_2}-\tau_0^{s_1})z}{2}\\+\frac{(\tau_0^{s_2}+\tau_0^{s_1})z^2}{2h_N+h_p}\end{pmatrix}dz,$$
(A.18)

$$G_{11N}^{*}=\int_{-h_N}^{h_N}\frac{\upsilon_N}{(1-\upsilon_N)}\begin{pmatrix}\frac{(\rho^{s_1}-\rho^{s_2})z}{2}\\-\frac{(\rho^{s_1}+\rho^{s_2})z^2}{2h_N+h_p}\end{pmatrix}dz,$$
$$G_{11p}^{*}=\int_{h_N}^{h_N+h_p}\frac{\upsilon_p}{(1-\upsilon_p)}\begin{pmatrix}\frac{(\rho^{s_1}-\rho^{s_2})z}{2}\\-\frac{(\rho^{s_1}+\rho^{s_2})z^2}{2h_N+h_p}\end{pmatrix}dz,$$
(A.19)

Note that, because of geometric symmetry, the expressions B_{ijN} is zero, i.e. $\big(B_{ijN}=0\big)$.

Appendix B

$$\alpha_1=\frac{1}{m_3}\bar{A}_{11},\ \alpha_2=\frac{m_0^2}{m_3}\bar{A}_{66},$$
$$\alpha_3=\frac{m_0}{m_3}(\bar{A}_{12}+\bar{A}_{21}),\alpha_4=\frac{2m_0}{m_3}\bar{A}_{66},$$
$$\alpha_5=\frac{m_0}{m_3}(\bar{A}_{12}+\bar{A}_{21}),$$
$$\alpha_6=\frac{1}{2m_1m_3}\big(2\bar{A}_{11}-\bar{\tau}_0^{s_1}-\bar{\tau}_0^{s_2}\big),$$
$$\alpha_7=\frac{m_0m_2}{2m_3}(\bar{A}_{12}+\bar{A}_{21}),\ \alpha_8=\frac{2m_0m_2}{m_3}\bar{A}_{66},$$
$$\alpha_9=\frac{m_0^2}{m_3}\bar{A}_{22},\alpha_{10}=\frac{m_0^2m_2}{2m_3}\big(2\bar{A}_{22}-\bar{\tau}_0^{s_1}-\bar{\tau}_0^{s_2}\big),$$
$$\alpha_{11}=\frac{m_2}{2m_3}(\bar{A}_{12}+\bar{A}_{21}),$$
$$\alpha_{12}=\frac{m_0^2}{m_3}\big(2\bar{A}_{22}-\bar{\tau}_0^{s_1}-\bar{\tau}_0^{s_2}\big),$$
$$\alpha_{13}=\frac{1}{m_3}\bar{A}_{66},\ \alpha_{14}=\frac{2m_2}{m_3}\bar{A}_{66},$$
$$\alpha_{15}=\frac{m_0^2}{m_3}\big(\bar{A}_{22}-\bar{\tau}_0^{s_1}-\bar{\tau}_0^{s_2}\big),$$
$$\alpha_{16}=\frac{1}{4m_1^2m_3}\big(\bar{A}_{11}-\bar{\tau}_0^{s_1}-\bar{\tau}_0^{s_2}\big),$$
$$\alpha_{17}=\frac{m_0^2m_2^2}{4m_3}\big(\bar{A}_{22}-\bar{\tau}_0^{s_1}-\bar{\tau}_0^{s_2}\big),$$
$$\alpha_{18}=\frac{m_2^2}{4m_3}(4\bar{A}_{66}+\bar{A}_{12}+\bar{A}_{21}),$$
$$\alpha_{19}=\frac{m_2}{2m_3}(\bar{A}_{12}+\bar{A}_{21}),$$
$$\alpha_{20}=\frac{m_0^2m_2}{m_3}\big(\bar{A}_{22}-\bar{\tau}_0^{s_1}-\bar{\tau}_0^{s_2}\big),$$
$$\alpha_{21}=-\frac{4m_0m_2}{m_3}\bar{B}_{66},$$
$$\alpha_{22}=\frac{m_0m_2}{m_3}(\bar{F}_{11}-\bar{B}_{12}-\bar{B}_{21}),$$
$$\alpha_{23}=\frac{1}{m_1m_3}(\bar{F}_{11}-2\bar{B}_{11}),$$

$$\alpha_{24}=\frac{m_2}{m_3}(\bar{F}_{11}-\bar{B}_{12}-\bar{B}_{21}),\alpha_{25}=-\frac{4m_2}{m_3}\bar{B}_{66},$$
$$\alpha_{26}=\frac{m_0^2m_2}{m_3}(\bar{F}_{11}-2\bar{B}_{22}),$$
$$\alpha_{27}=\frac{m_2^2}{2m_3}(\bar{F}_{11}-\bar{B}_{12}-\bar{B}_{21}),$$
$$\alpha_{28}=\frac{m_2}{m_3}(\bar{F}_{11}-\bar{B}_{12}-\bar{B}_{21}),$$
$$\alpha_{29}=\frac{m_2^2}{2m_3}(\bar{F}_{11}-\bar{B}_{12}-\bar{B}_{21}),$$
$$\alpha_{30}=\frac{1}{2m_1^2m_3}\left(\bar{F}_{11}-2\bar{B}_{11}+\bar{\tau}_0^{s_2}(1+m_4)-\bar{\tau}_0^{s_1}\right),$$
$$\alpha_{31}=\frac{m_0^2m_2^2}{2m_3}\left(\bar{F}_{11}-2\bar{B}_{22}+\bar{\tau}_0^{s_2}(1+m_4)-\bar{\tau}_0^{s_1}\right),$$
$$\alpha_{32}=-\frac{4m_2^2}{m_3}\bar{B}_{66},$$
$$\alpha_{33}=\frac{m_0^2m_2}{m_3}\left(\bar{F}_{11}-2\bar{B}_{22}+\bar{\tau}_0^{s_2}(1+m_4)-\bar{\tau}_0^{s_1}\right),$$
$$\alpha_{34}=\frac{1}{m_1^2m_3}(\bar{D}_{11}-\bar{E}_{11}),$$
$$\alpha_{35}=\frac{m_0^2m_2^2}{m_3}(\bar{D}_{22}-\bar{E}_{11}),\ \alpha_{36}=\frac{4m_2^2}{m_3}\bar{D}_{66},$$
$$\alpha_{37}=\frac{m_2^2}{m_3}(\bar{D}_{12}+\bar{D}_{21}-2\bar{E}_{11}),$$
$$\alpha_{38}=\frac{m_0m_1}{m_3}\left(\bar{\tau}_0^{s_1}+\bar{\tau}_0^{s_2}-\bar{N}_{\theta p}\right),$$
$$\alpha_{39}=\frac{m_1}{m_3}\left(\bar{\tau}_0^{s_1}+\bar{\tau}_0^{s_2}-\bar{N}_{xp}\right),$$
$$\alpha_{40}=\frac{m_0m_1}{m_3}\left(\bar{\tau}_0^{s_1}+\bar{\tau}_0^{s_2}-\bar{N}_{\theta p}\right),$$
$$\alpha_{41}=\frac{1}{2m_3}\left(\bar{\tau}_0^{s_1}+\bar{\tau}_0^{s_2}-\bar{N}_{xp}\right),$$
$$\alpha_{42}=\frac{m_0^2}{2m_3}\left(\bar{\tau}_0^{s_1}+\bar{\tau}_0^{s_2}-\bar{N}_{\theta p}\right),$$
$$\alpha_{43}=\frac{1}{m_3}(\bar{M}_{xp}+\bar{\tau}_0^{s_1}-\bar{\tau}_0^{s_2}(1+m_4)),$$
$$\alpha_{44}=\frac{m_0^2}{m_3}\left(\bar{M}_{\theta p}+\bar{\tau}_0^{s_1}-\bar{\tau}_0^{s_2}(1+m_4)\right),$$
$$\alpha_{45}=-\frac{1}{2m_1^2m_3}\bar{G}_{11}^*,\alpha_{46}=-\frac{m_2^2}{2m_3}\bar{G}_{11}^*,$$
$$\alpha_{47}=\frac{1}{2m_1m_3}\bar{J}_{11}^*,\alpha_{48}=\frac{m_2}{2m_3}\bar{J}_{11}^*,$$
$$\alpha_{49}=\frac{m_2}{2m_3}\bar{J}_{11}^*,\alpha_{50}=\frac{1}{4m_1^2m_3}\bar{J}_{11}^*,\alpha_{51}=\frac{m_2^2}{4m_3}\bar{J}_{11}^*,$$

Appendix C

$$(M)_u^u=\iint\left(\chi_e\chi_i\vartheta_f\vartheta_j\right)d\xi d\theta\ ,$$

$$(M)_u^w=\frac{1}{2}\alpha_{47}\iint\left(\chi_{\mathrm{e}}'\beta_o\vartheta_f\psi_l\right)d\xi d\theta$$

$$(K)_u^u=\iint\left(\alpha_1\chi_{\mathrm{e}}'\chi_{\mathrm{i}}'\vartheta_f\vartheta_j+\alpha_2\chi_e\chi_i\vartheta_f'\vartheta_j'\right)d\xi d\theta\ ,$$

$$(K)_u^v=\frac{1}{2}\iint\left(\alpha_3\chi_{\mathrm{e}}'\phi_k\vartheta_f\alpha_l'+\alpha_4\chi_e\phi_k'\vartheta_f'\alpha_l\right)d\xi d\theta$$

$$(K)_u^w=$$
$$\frac{1}{2}\iint\begin{pmatrix}\alpha_5\chi_{\mathrm{e}}'\beta_o\vartheta_f\psi_l+\alpha_{21}\chi_e\beta_0'\vartheta_f'\psi_l'\\+\alpha_{22}\chi_{\mathrm{e}}'\beta_o\vartheta_f\psi_l''+\alpha_{23}\chi_{\mathrm{e}}'\beta_0''\vartheta_f\psi_l\end{pmatrix}d\xi d\theta$$

$$(NL)_u^w=\frac{1}{2}\iint\begin{pmatrix}\alpha_6\chi_{\mathrm{e}}'\beta_0'\beta_t'\vartheta_f\psi_p\psi_v\\+\alpha_7\chi_{\mathrm{e}}'\beta_o\beta_t\vartheta_f\psi_p'\psi_v'\\+\alpha_8\chi_e\beta_0'\beta_t\vartheta_f'\psi_p\psi_v'\end{pmatrix}d\xi d\theta$$

$$\bar{F}_{up}=\frac{1}{2}\alpha_{39}\iint(\chi_{\mathrm{e}}'\vartheta_i)d\xi d\theta\ ,$$

$$(M)_v^v=\iint\left(\phi_q\phi_k a_f a_l\right)d\xi d\theta\ ,$$

$$(M)_v^w=\frac{1}{2}\alpha_{48}\iint\left(\phi_q\beta_o\alpha_f'\psi_l\right)d\xi d\theta$$

$$(K)_v^u=\frac{1}{2}\iint\left(\alpha_3\phi_q\chi_{\mathrm{i}}'\alpha_f'\vartheta_l+\alpha_4\phi_q'\chi_i\alpha_f\vartheta_l'\right)d\xi d\theta\ ,$$

$$(K)_v^v=\iint\left(\alpha_9\phi_q\phi_k\alpha_f'\alpha_l'+\alpha_{13}\phi_q'\phi_k'\alpha_f\alpha_l\right)d\xi d\theta$$

$$(K)_v^w=$$
$$\frac{1}{2}\iint\begin{pmatrix}\alpha_{12}\phi_q\beta_o\alpha_f'\psi_l+\alpha_{24}\phi_q\beta_0''\alpha_f'\psi_l\\+\alpha_{25}\phi_q'\beta_0'\alpha_f\psi_l'+\alpha_{26}\phi_q\beta_o\alpha_f'\psi_l''\end{pmatrix}d\xi d\theta$$

$$(NL)_v^w=\frac{1}{2}\iint\begin{pmatrix}\alpha_{10}\phi_q\beta_o\beta_t\alpha_g'\psi_p'\psi_v'\\+\alpha_{11}\phi_q\beta_0'\beta_t'\alpha_g'\psi_p\psi_v\\+\alpha_{14}\phi_q'\beta_0'\beta_t\alpha_g\psi_p\psi_v'\end{pmatrix}d\xi d\theta$$

$$\bar{F}_{vp}=\frac{1}{2}\alpha_{40}\iint\left(\phi_q\alpha_f'\right)d\xi d\theta$$

$$(M)_w^w=$$
$$\frac{1}{2}\iint\begin{pmatrix}2\beta_r\beta_o\psi_s\psi_p+\alpha_{45}\beta_r''\beta_o\psi_s\psi_p\\+\alpha_{46}\beta_r\beta_o\psi_s''\psi_p+\alpha_{49}\beta_r\beta_o\psi_s\psi_p\\+\bar{\rho}_1\beta_r\beta_o\psi_s\psi_p\end{pmatrix}d\xi d\theta$$

$$(C)_w^w=$$
$$\frac{1}{2}\iint\begin{pmatrix}\bar{C}_w\beta_r\beta_o\psi_s\psi_p+\bar{\rho}_2\beta_r\beta_o'\psi_s\psi_p\\-\bar{\mu}_1\beta_r\beta_o''\psi_s\psi_p-\bar{\mu}_2\beta_r\beta_o\psi_s\psi_p''\end{pmatrix}d\xi d\theta$$

$$(K)_w^u=$$

$$\frac{1}{2}\iint \begin{pmatrix} \alpha_5\beta_r\chi_{\mathrm{i}}'\psi_s\vartheta_j + \alpha_{21}\beta_r'\chi_i\psi_p'\vartheta_j' \\ +\alpha_{22}\beta_r\chi_{\mathrm{i}}'\psi_s''\vartheta_j + \alpha_{23}\beta_r''\chi_{\mathrm{i}}'\psi_s\vartheta_j \end{pmatrix} d\xi d\theta$$

$$(K)_w^v =$$

$$\frac{1}{2}\iint \begin{pmatrix} \alpha_{12}\beta_r\phi_k\psi_s\alpha_l' + \alpha_{24}\beta_r''\phi_k\psi_s\alpha_l' \\ +\alpha_{25}\beta_r'\phi_k'\psi_s'\alpha_l + \alpha_{26}\beta_r\phi_k\psi_s''\alpha_l' \end{pmatrix} d\xi d\theta$$

$$(K)_w^w =$$

$$\frac{1}{2}\iint \begin{pmatrix} 2\alpha_{15}\beta_r\beta_o\psi_s\psi_p + \alpha_{28}\beta_r\beta_0''\psi_s\psi_p \\ +\alpha_{28}\beta_r''\beta_o\psi_s\psi_p + \alpha_{33}\beta_r\beta_o\psi_s\psi_p'' \\ +\alpha_{33}\beta_r\beta_o\psi_s''\psi_p + 2\alpha_{34}\beta_r''\beta_0''\psi_s\psi_p \\ +2\alpha_{35}\beta_o\beta_r\psi_s''\psi_p'' + 2\alpha_{36}\beta_r'\beta_o'\psi_s'\psi_p' \\ +\alpha_{37}\beta_r\beta_o''\psi_s''\psi_p + \alpha_{37}\beta_r''\beta_o\psi_s\psi_p'' \\ +2\alpha_{41}\beta_r'\beta_o'\psi_s\psi_p + 2\alpha_{42}\beta_r\beta_o\psi_s'\psi_p' \\ +\bar{k}_w\beta_r\beta_o\psi_s\psi_p - \bar{k}_p\beta_r\beta_0''\psi_s\psi_p \\ -\bar{k}_p m_0^2\beta_r\beta_o\psi_s\psi_p'' + \bar{\rho}_3\beta_r\beta_0''\psi_s\psi_p \\ -\bar{\mu}_3\beta_r\beta_0'''\psi_s\psi_p - \bar{\mu}_4\beta_r\beta_0'\psi_s\psi_p'' \\ -\bar{F}_{e2}(K_e)_w^w \end{pmatrix} d\xi d\theta$$

$$(K_e)_w^w = \beta_r\beta_o\psi_s\psi_p,$$

$$(K)_{w2}^{\ddot{w}} = \iint \begin{pmatrix} \alpha_{50}\beta_r'\beta_o\beta_t'\psi_s\psi_p\psi_v \\ +\alpha_{51}\beta_r\beta_o\beta_t\psi_s'\psi_p\psi_v' \end{pmatrix} d\xi d\theta$$

$$(NL)_w^u = \frac{1}{2}\iint \begin{pmatrix} 2\alpha_6\beta_r'\beta_o'\chi_{\mathrm{i}}'\psi_s\psi_p\vartheta_j \\ +2\alpha_7\beta_r\beta_o\chi_{\mathrm{i}}'\psi_s'\psi_p'\vartheta_j \\ +\alpha_8\beta_r'\beta_o\chi_i\psi_s\psi_p'\vartheta_j' \\ +\alpha_8\beta_r\beta_o'\chi_i\psi_s'\psi_p\vartheta_j' \end{pmatrix} d\xi d\theta$$

$$(NL)_w^v = \frac{1}{2}\iint \begin{pmatrix} 2\alpha_{10}\beta_r\beta_o\phi_k\psi_s'\psi_p'\alpha_l' \\ +2\alpha_{11}\beta_r'\beta_o'\phi_k\psi_s\psi_p\alpha_l' \\ +\alpha_{14}\beta_r'\beta_o\phi_k'\psi_s\psi_p'\alpha_l \\ +\alpha_{14}\beta_r\beta_o'\phi_k'\psi_s'\psi_p\alpha_l \end{pmatrix} d\xi d\theta$$

$$(NL)_{w2}^w = \frac{1}{2}\iint \begin{pmatrix} \alpha_{19}\beta_r\beta_o'\beta_t'\psi_s\psi_p\psi_v \\ +2\alpha_{19}\beta_r'\beta_o'\beta_t\psi_s\psi_p\psi_v \\ +\alpha_{20}\beta_r\beta_o\beta_t\psi_s\psi_p'\psi_v' \\ +2\alpha_{20}\beta_r\beta_o\beta_t\psi_s'\psi_p'\psi_v \\ +\alpha_{27}\beta_r''\beta_o\beta_t\psi_s\psi_p'\psi_v' \\ +2\alpha_{27}\beta_r\beta_o\beta_t''\psi_s'\psi_p'\psi_v \\ +\alpha_{29}\beta_r\beta_o'\beta_t'\psi_s''\psi_p\psi_v \\ +2\alpha_{29}\beta_r'\beta_o'\beta_t\psi_s\psi_p\psi_v'' \\ +\alpha_{30}\beta_r''\beta_o'\beta_t'\psi_s\psi_p\psi_v \\ +2\alpha_{30}\beta_r'\beta_o'\beta_t''\psi_s\psi_p\psi_v \\ +\alpha_{31}\beta_r\beta_o\beta_t\psi_s''\psi_p'\psi_v' \\ +2\alpha_{31}\beta_r\beta_o\beta_t\psi_s'\psi_p'\psi_v'' \\ +\alpha_{32}\beta_r'\beta_o'\beta_t\psi_s'\psi_p\psi_v' \\ +\alpha_{32}\beta_r'\beta_o'\beta_t\psi_s\psi_p'\psi_v' \\ +\alpha_{32}\beta_r\beta_o'\beta_t'\psi_s'\psi_p\psi_v' \\ -\bar{F}_{e3}(NL_{2e})_w^w \end{pmatrix} d\xi d\theta$$

$$(NL_{2e})_w^w = \beta_r\beta_o\beta_t\psi_s\psi_p\psi_v$$

$$(NL)_{w3}^w =$$

$$\frac{1}{2}\iint \begin{pmatrix} 4\alpha_{16}\beta_r'\beta_o'\beta_t'\beta_a'\psi_s\psi_p\psi_v\psi_b \\ +4\alpha_{17}\beta_r\beta_o\beta_t\beta_a\psi_s'\psi_p'\psi_v'\psi_b' \\ +2\alpha_{18}\beta_r'\beta_o'\beta_t\beta_a\psi_s\psi_p\psi_v'\psi_b' \\ +2\alpha_{18}\beta_r\beta_o\beta_t'\beta_a'\psi_s'\psi_p'\psi_v\psi_b \\ -\bar{F}_{e4}(NL_{3e})_w^w \end{pmatrix} d\xi d\theta$$

$$(NL_{3e})_w^w = \beta_r\beta_o\beta_t\beta_a\psi_s\psi_p\psi_v\psi_b$$

$$\bar{F}_{wp} = \frac{1}{2}\iint \begin{pmatrix} \alpha_{38}\beta_r\psi_s + \alpha_{43}\beta_r''\psi_s \\ +\alpha_{44}\beta_r\psi_s'' \end{pmatrix} d\xi d\theta$$

$$\bar{F}_1 = \iint (\beta_r\psi_s) d\xi d\theta \ , \bar{F}_{e1} = \bar{F}_e\bar{F}_1,$$

$$\bar{F}_{eDC} = \bar{F}_e\bar{V}_{DC}^2, \bar{F}_{we} = \frac{1}{2}\bar{C}_1\bar{F}_{eDC}\bar{F}_1,$$

$$\bar{F}_{e2} = \bar{C}_2\bar{F}_{eDC}, \bar{F}_{e3} = \bar{C}_3\bar{F}_{eDC}, \bar{F}_{e4} = \bar{C}_4\bar{F}_{eDC},$$

References:

[1] Chatterjee, K., Sarkar, S., Rao K. J. and Paria, S., Core/shell nanoparticles in biomedical applications, *Advances in Colloid and Interface Science*, Vol.209, 2014, pp.8–39.

[2] Melancon, M. P., Lu, W., Zhong, M., Zhou, M., Liang, G., Elliott, A. M., Hazle, J.D., Myers, J. N., Li, C. and Stafford R. J., Targeted multifunctional gold-based nanoshells for magnetic natural-guided laser ablation of head and neck cancer, *Biomaterials*. Vol. 32 No.30, 2011, pp. 7600–7608.

[3] Riley, R. S., O'Sullivan, R. K., Potocny, A.M., Rosenthal, J. and Day, E. S., Evaluating Nanoshells and a Potent Biladiene Photosensitizer for Dual Photothermal and Photodynamic Therapy of Triple Negative Breast Cancer Cells, *Nanomaterials*, doi:10.3390/nano8090658, 2018.

[4] Sobral-Filho, R. G., Brito-Silva, A. M., Isabelle, M., Jirasek, A., Lum, J. J. and Brolo A. G., Plasmonic labeling of subcellular compartments in cancer cells: multiplexing with fine-tuned gold and silver nanoshells, *Chemical Science*, Vol. 8, 2017, pp. 3038–3046.

[5] Ayala-Orozco, C., Urban, C., Knight, M. W., Urban, A. S., Neumann, O., Bishnoi, S. W., Mukherjee, S., Goodman, A. M., Charron, H., Mitchell, T., Shea, M., Roy, R., Nanda, S., Schiff, R., Halas, N. J. and Joshi, A., Au Nanomatryoshkas as Efficient Near-Infrared Photothermal Transducers for Cancer

Treatment: Benchmarking against Nanoshells, *ACS Nano*. Vol. 8, No. 6, 2014, pp. 6372-81.

[6] Choi, Y.E., Kwak, J.W. and Park, J. W., Nanotechnology for Early Cancer Detection, Vol. 10, 2010, pp.428-455.

[7] Singhana, B., Slattery, P., Chen, A., Wallace, M. and Melancon, M. P., Light-Activatable Gold Nanoshells for Drug Delivery Applications, *AAPS PharmSciTech*, Vol. 15 No.3, 2014, pp. 741–752.

[8] Riley, R.S., Day, E.S., Gold nanoparticle-mediated photothermal therapy: Applications and opportunities for multimodal cancer treatment, *Wiley Interdisciplinary Reviews Nanomedicine and Nanobiotechnology*, DOI:10.1002/wnan.1449, 2017.

[9] Eloy, J.O., Petrilli, R., Lopez, R.F.V. and Lee, R.J., Stimuli-responsive nanoparticles for siRNA delivery, *Current Pharmaceutical Design*, Vol.21, 2015, pp. 4131–4144.

[10] Li, C., Thostenson, E. T. and Chou, T.W., Sensors and actuators based on carbon nanotubes and their composites: A review, *Composites Science and Technology*, Vol. 68, 2008, pp.1227–1249.

[11] Mousavi, S. M., Hashemi, S. A., Zarei, M., Amani, A. M. and Babapoor, A., Nanosensors for Chemical and Biological and Medical Applications, *Medicinal Chemistry*, Vol. 8 No. 8, 2018, pp.205-217.

[12] Mosayebi, R., Ahmadzadeh, A., Wicke, W., Jamali, V., Schober, R. and Nasiri-Kenari, M., Early Cancer Detection in Blood Vessels Using Mobile Nanosensors, *arXiv*,1805.08777, 2018.

[13] Kosaka, P. M., Pini, V., Ruz, J. J., da Silva, R. A., González, M. U., Ramos, D., Calleja, M. and Tamayo, J., Detection of cancer biomarkers in serum using a hybrid mechanical and optoplasmonic nanosensors, *Nature Nanotechnology*, DOI: 10.1038/NNANO.2014.250, 2014.

[14] Aspinwall, C. A., Nanoshell sensors for cellular analysis, *National Institute of Health (NIH), Project number*: 5R01GM116946-042019, 2019.

[15] Duan, W. H., Wang, Q. and Quek, S.T., Applications of Piezoelectric Materials in Structural Health Monitoring and Repair: Selected Research Examples, *Materials*, Vol.3, 2010, pp.5169-5194.

[16] Rupitsch, S. J., *Piezoelectric Sensors and Actuators: Fundamentals and Applications*, Springer, New York, 2019.

[17] Jalili, N., *Piezoelectric-Based Vibration Control: From Macro to Micro/Nano Scale Systems*, Springer, New York, 2010.

[18] Gurtin, M.E. and Murdoch, A.I., A continuum theory of elastic material surface, *Archive for Rational Mechanics and Analysis*, Vol.57 No.4, 1975, pp. 291–323.

[19] Gurtin, M.E. and Murdoch, A.I., Surface stress in solids, *International Journal of Solids and Structures*, Vol.14 No.6, 1978, pp. 431–40.

[20] Zhu, C.S., Fang, X.Q. and Liu, J.X., Surface energy effect on buckling behavior of the functionally graded nano-shell covered with piezoelectric nano-layers under torque, *International Journal of Mechanical Sciences*, Vol.133, 2017, pp. 662–673.

[21] Fang, X.Q., Zhu, C.S. and Liu, J.X., Surface energy effect on free vibration of nano-sized piezoelectric double-shell structures, *Physica B: Condensed Matter*, Vol. 529 No.15, 2018, pp.41-56.

[22] Ghorbanpour Arani, A., Amir, S., Dashti, P. and Yousefi M., Flow-induced vibration of double bonded visco-CNTs under magnetic fields considering surface effect, *Computational Materials Science*, Vol.86, 2014, pp.144–154.

[23] Ghorbanpour Arani, A., Kolahchi, R. and Hashemian, M., Nonlocal surface piezoelasticity theory for dynamic stability of double-walled boron nitride nanotube conveying viscose fluid based on different theories, *Proceedings of the Institution of Mechanical Engineers, Part C: Journal of Mechanical Engineering*, Vol.228 No.17, 2014, pp.3258-3280.

[24] Fereidoon, A., Andalib, E. and Mirafzal, A., Nonlinear Vibration of Viscoelastic Embedded-DWCNTs Integrated with Piezoelectric Layers-Conveying Viscous Fluid Considering Surface Effects, *Physica E: Low-Dimensional Systems and Nanostructures*, Vol.81, 2016, pp. 205–218.

[25] Ansari, R., Gholami, R., Norouzzadeh, A. and M. A. Darabi, Surface Stress Effect on the Vibration and Instability of Nanoscale Pipes Conveying Fluid Based on a Size-Dependent Timoshenko Beam Model, *Acta Mechanica Sinica*, Vol.31, 2015, pp. 708-719.

[26] Ye, T., Jin, G., Chen, Y., Ma, X. and Su, Z., Free vibration analysis of laminated composite shallow shells with general elastic boundaries, *Composite Structures*, Vol.106, 2013, pp. 470–490.

[27] Fazzolari, F.A., A refined dynamic stiffness element for free vibration analysis of cross-ply laminated composite cylindrical and spherical shallow shells, *Composite Structures, Part B*, Vol.62, 2014, pp.143–158.

[28] Mirza, S. and Alizadeh, Y., Free vibration of partially supported cylindrical shells, *Shock and Vibration*, Vol.2 No. 4, 1995, pp.297–306.

[29] Loy, C.T., Lam, K.Y. and Shu, C., Analysis of cylindrical shells using generalized differential quadrature, *Shock and Vibration*, Vol.4 No.3, 1997, pp.193–198.

[30] Naeem, M.N. and Sharma, C.B., Prediction of natural frequencies for thin circular cylindrical shells, *Proceedings of the Institution of Mechanical Engineers Part C: Journal of Mechanical Engineering Science*, Vol.214 No.10, 2000, pp.1313–1328.

[31] Zeighampour, H., Tadi Beni, Y. and Botshekanan, D. M., Wave propagation in viscoelastic thin cylindrical nanoshell resting on a visco-Pasternak foundation based on nonlocal strain gradient theory, *Thin-Walled Structures*, Vol.122, 2018, pp. 378–386.

[32] Donnell, L. H., *Beam, Plates and Shells*, McGraw-Hill, New York, 1976.

[33] Amabili, M., *Nonlinear Vibrations and Stability of Shells and Plates*, Cambridge University Press, New York, 2008.

[34] Sabzikar Boroujerdy, M. and Eslami, M.R., Axisymmetric snap-through behavior of Piezo-FGM shallow clamped spherical shells under thermo-electro-mechanical loading, *International Journal of Pressure Vessels and Piping*, Vol.120-121, 2014, pp. 19-26.

[35] Kirchhoff, G., Über das Gleichgewicht und die Bewegung einer elastischen Scheibe, *Journal fur reine und angewandte Mathematik*, Vol.40, 1850, pp.51-88.

[36] Lu, P., He, L.H., Lee, H.P. and Lu, C., Thin plate theory including surface effects, *International journal Solids and Structure*, Vol.43 No.16, 2006, pp. 4631–47.

[37] Ghorbanpour Arani, A., Kolahchi, R. and Hashemian M., Nonlocal surface piezoelasticity theory for dynamic stability of double-walled boron nitride nanotube conveying viscose fluid based on different theories, *Proceedings of the Institution of Mechanical Engineers, Part C: Journal of Mechanical Engineering Science*, DOI: 10.1177/0954406214527270, 2014.

[38] Ghorbanpour Arani, A., Amir, S., Shajari, A.R. and Mozdianfard, M.R., Electro-thermo-mechanical buckling of DWBNNTs embedded in bundle of CNTs using nonlocal piezoelasticity cylindrical shell theory, *Composites: Part B*, Vol. 43, 2012, pp.195–203.

[39] Farokhi, H., Païdoussis, M.P. and Misra, A., A new nonlinear model for analyzing the behaviour of carbon nanotube-based resonators, *Journal of Sound and Vibration*, Vol. 378, 2016, pp. 56-75.

[40] Wang, L. and Ni, Q., A reappraisal of the computational modelling of carbon nanotubes conveying viscous fluid, *Mechanics Research Communications*, Vol.36, 2009, pp.833–837.

[41] Reddy, J.N. and Wang, C.M., Dynamics of fluid-conveying beams: governing equations and finite element models, *Centre for Offshore Research and Engineering National University of Singapore*, Core report No. 2004-03, 2004.

[42] Jafari, A.A., Khalili, S.M.R. and Tavakolian, M., Nonlinear vibration of functionally graded cylindrical shells embedded with a piezoelectric layer, *Thin Wall Structures*, Vol.79, 2014, pp.8–15.

[43] Mohammadimehr, M. and Rostami R., Bending and vibration analyses of a rotating sandwich cylindrical shell considering nanocomposite core and piezoelectric layers subjected to thermal and magnetic fields, *Applied Mathematics and Mechanics*, Vol.39 No. 2, 2018, pp.1-22.

[44] Lide, D. R., *CRC Handbook of Chemistry and Physics (86th Edition)*. Boca Raton (FL): CRC Press (an imprint of Taylor and Francis Group): Boca Raton, F.L., 2005, 2544 pp.